Constraining Hydrodynamics on Plesiosaur Locomotion

by

Ali Pourfarzan

A thesis submitted in partial fulfillment of the requirements for the degree of

Master of Science

Department of Mechanical Engineering
University of Alberta

© Ali Pourfarzan, 2022

Abstract

Plesiosaurs were a diverse group of Mesozoic marine reptiles, notable among both extinct and extant animals for their unique body planform. Despite being known for more than 300 years, many aspects of their locomotion and behavior remain as mystery. Unlike any other flapping species, plesiosaurs exhibit two pairs of near-identical wing-like flippers, which have remained consistent throughout their evolution. Despite the similarity in geometry between fore and hind flippers, their morphologies have been identified to be slightly different. This has given rise to contradicting hypotheses on locomotion and their behavior. In particular, the role of the hind flipper and the relative motion of the flippers have been questioned. In this thesis, which consists of two research chapters, two different approach are considered to address these questions. First, by using universal scaling laws, it is shown that the group of plesiosaurs with short necks and large heads, known as pliosauroids, likely had a high agility level, possibly similar to penguins, while long-necked, small-headed plesiosaurs (plesiosauroids) likely had limited agility, possibly similar to that observed in sea turtles. Second, through a series of particle image velocimetry experiments on the effect of varying amplitude ratio on tandem oscillating foils, it is demonstrated that plesiosaurs utilizing rear-biased and equal amplitude propulsion, could have achieved higher thrust production and propulsive efficiency. However, the rear-biased model is found to be more efficient with slightly higher thrust production. This strategy may have been utilized by pliosauroids, known to be pursuit predators, as it is consistent with fossil records, with joints of the hind flipper accommodating greater flapping angles. It is possible that this strategy was also used by plesiosauroids for high thrust production such as during escape, however it is inconsistent with fossil measurements. The findings of this work suggest that amplitude ratio, along with

other important parameters such as varying the phase differential of flipper oscillation and inter-foil spacing, was a critical optimizing parameter for the propulsive performance of a tandem-flipper propulsor.

Preface

This thesis is written in compilation form. Central chapters of this thesis consist of multi-authored work. The contributions of each co-author is provided as below:

Chapter 2 of this thesis with the title of "Fluid dynamics, scaling laws and plesiosaur locomotion" has been submitted to *Bioinspiration & Biomimetics*, and currently, the manuscript is being revised and prepared for a second round of review. I collected the kinematic data of species, reconstructed 3D skeletons of sea turtles, analyzed the data. Dr. Henderson contributed via generating 3D plesiosaur models and computing spans of plesiosaur and sea turtle flippers and reviewing drafts of text. Dr. Wong designed and supervised the study and reviewed drafts of the text. All authors contributed to writing the manuscript.

Chapter 3 of this thesis has been submitted to *Physics of Fluids* and currently is in press:

1. Pourfarzan, Ali, Wong, Jaime G. (2022) Constraining optimum swimming strategies in plesiosaurs: The effect of amplitude ratio on tandem pitching foils. *Physics of Fluids*. (In press)

I personally conducted the experiments, analyzed data, and wrote the manuscript. Dr. Wong supervised the work, reviewed and edited the drafts of the text.

It should be noted that Chapters 2 and 3 appear exactly as they are submitted to the journals excluding citation style, which is altered to adhere to the structure of the thesis. As the articles are not published at this moment, co-authors and I are the copyright holders.

Dedicated to my parents, Zahra Sadrkabir and Iraj Pourfarzan

Acknowledgements

I would like to express my deepest gratitude to Dr. Jaime Wong for giving me this opportunity to work under his supervision. I deeply appreciate his patience in supporting me and sharing his knowledge and expertise for the challenges I had throughout this project. His enthusiasm for science and dedication to work has instilled invaluable attributes in me, which I will carry lifelong.

I would also like to express my appreciation to Dr. Donald Henderson at Royal Tyrell Museum, for guiding me through the fascinating world of paleontology and for his contributions to this work. I must also thank Dr. Sina Ghaemi for allowing me to conduct my experiments in his laboratory and using his research facilities.

Finally, I am extremely grateful to my parents, my sister and friends for always being there for me and supporting me in reaching my goals. I owe it to you all!

Contents

List of Tables

List of Figures

Chapter 1

Introduction

During the "Age of Dinosaurs", plesiosaurs were one of the most successful marine reptile clades. They were the dominant aquatic animals and widely spread in the oceans from the Late Triassic (Benson et al., 2012; Wintrich et al., 2017) up to the end of the Cretaceous (Allemand et al., 2018) from about 200 to 66 million years ago. Plesiosaurs are known for their unique body planforms among extinct and existing animals as they exhibit four wing-like flippers of similar geometry and size. Although the body size and neck length evolved through millions of years within the clade, the similarity between the fore and hind flippers of the specimens has remained consistent. This is indicative of the importance of this characteristic for plesiosaurs' survival. However, in the absence of a living analogue exhibiting such flippers, there have been contradictory hypotheses on the role of each set of flippers in locomotion. Sea turtles, penguins and sea lions are some examples that exhibit four propulsive limbs, however, unlike plesiosaurs, the limbs take very different forms. In these animals, while the hydrofoil shaped fore flippers are used for thrust generation, the hind flippers are utilized for steering. Apart from the similarity in the flippers' size and shape, the difference in morphology observed in the limbs have steered debates on their swimming behavior. Were the fore flippers employed to generate thrust while the hind flippers were used for steering, as seen in sea turtles and penguins? Which flipper set was dominant in thrust generation? Were they agile enough to chase smaller prey? How does the difference in morphology between the fore and hind flippers affect their swimming behavior? Answering these questions can help paleontologists understand plesiosaurs' likely behavior and hunting style. For example, knowing a plesiosaur's swimming behavior and maneuverability level can be an effective way to determine which animals it may have predated, thus revealing its

likely place in the prehistoric food chain.

Meanwhile, bio-inspired locomotion has received much interest in the recent years, as understanding natural swimming and flying behavior of animals can provide insight into similar engineered problems. Natural flyers and swimmers have extremely high performance in low speed flying and swimming regimes. Therefore, knowledge acquired by investigating their locomotion can be employed to design and manufacture more efficient marine and aerial propulsors. Plesiosaur flippers very much resemble efficient hydrofoils, and hence it is reasonable to abstract them as tandem flapping foils (Robinson, 1975; Muscutt et al., 2017b). Recently, it has been shown that tandem propulsors achieve to high thrust and high efficiency concurrently (Boschitsch et al., 2014; Muscutt et al., 2017a; Joshi and Mysa, 2021), demonstrating their potential superiority compared to single flipper or foil propulsors, which generate high thrust at the cost of higher power consumption and lower efficiency. As plesiosaurs are an exceptional example among flapping animals, understanding their locomotion offers an excellent opportunity to further enhance the current knowledge in the field of natural propulsion, and in particular, oscillating tandem propulsors.

As this work is at the interface of engineering and biology, the goal of this chapter will be to summarize plesiosaur anatomy and the hypotheses on plesiosaur locomotion as discussed in both the paleontology and engineering literature, in order to be accessible to readers from either field. The evolutionary convergence in aerodynamic and hydrodynamic performance of natural flyers and swimmers will be briefly discussed as well. Further, a brief review on flapping propulsion and its abstraction as single and tandem flapping foils in the engineering world will be provided. Finally, the contribution of current thesis will be outlined in relation to existing studies of plesiosaur swimming and tandem flapping propulsion.

1.1 Plesiosauria

Plesiosaurs were marine reptiles which that were first discovered in 1719 (Stukeley, 1719). As secondarily marine tetrapods, plesiosaurs were ocean-going and air-breathing carnivorous reptiles. They were considered as one of the extremely successful clades not just because of their distribution across the prehistoric seas and oceans in the world, but due to their persistence through different stages of Mesozoic Era (Henderson, 2006). They are generally known for their peculiar body planform: snake-like necks, turtle-like trunks, and wing-like

flippers! Throughout their evolution their body plan and size evolved several times, forming a diverse clade of marine reptiles with more than 120 valid genera (Fischer et al., 2018). Previously, plesiosaurs were classified based on neck length, head and flipper sizes. According to this taxonomy, plesiosaurs with long necks, small heads and small flippers were grouped as Plesiosauroidea (plesiosauroids), and plesiosaurs with short necks, large heads, and large flippers were known as Pliosauroidea (pliosauroids) (Figure 1.1). Relating the body proportions to trophic specialization, it was argued that plesiosauroids were ambush predators, while pliosauroids as were likely pursuit predators, were chasing their preys Taylor (1981); Massare (1988). Later O'Keefe (2002) casted doubt on the validity of this classification, arguing that this is an oversimplification of the diversity of morphologies observed within the clade. It was suggested that specimens with extreme morphologies have become apparent due to long-term evolution, where intermediate morphologies disappear as a result of more derivation. However, in the current thesis, for the purpose of the simplicity, classical dichotomy of long-necked, small-headed plesiosaurs (plesiosauroids) and short-necked, large-headed plesiosaurs (pliosauroids) will be used to address the discussions related to the specimens exhibiting these morphological specifications.

1.1.1 Flipper and Girdle Anatomy

Plesiosaur limbs had evolved into hydrofoil-like flippers, which are tapered towards the tip with cambered crossed section (Robinson, 1975, 1977). This observation by Robinson (1975), resulted in a hypothesis that plesiosaurs were under-water flyers, which will be discussed in detail next section, but for the purpose of introduction, it is a mode of propulsion that utilizes lift rather than drag. Due to their terrestrial ancestors, plesiosaur flippers had tetropod morphology. The components of the fore flippers are humerus, ulna and radius, carpals, metacarpals, and phalanges (see Figure 1.2). Respective components in hind flippers are femur, tibia and fibula, tarsals, metatarsals, and phalanges.

Plesiosaur flippers show extreme hyperphalangy as they exhibit large number of phalanges. It was suggested that hyperphalangy would have resulted in smoother bending than flippers with fewer and longer phalanges to obtain hydrodynamic advantage (Cooper et al., 2007). Krahl (2021) suggested that hyperphalangy might have increased the possibility of flipper twisting, especially if the flippers had a limited capacity for pronation-supination motion (long axis rotation) similar to sea turtles.

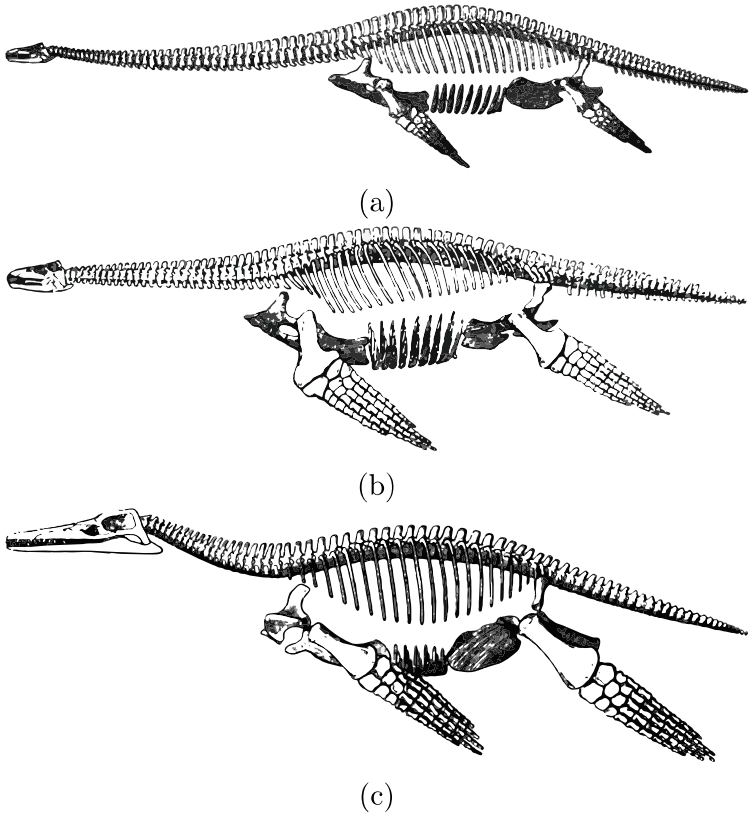

Figure 1.1: Plesiosaurs with different body proportions. Reproduced from Muscutt (2017). Original caption: Examples of three plesiosaurs of different morphologies. (a) *Muraenosaurus leedsii* (b) *Cryptocleidus oxoniensis* (c) *Peloneustes philarchus* redrawn from Andrews (1913))

Humeri (in fore flippers) and femurs (in hind flippers) are proximal elements of the flippers which have rounded proximal heads and are attached to the articular sockets on the

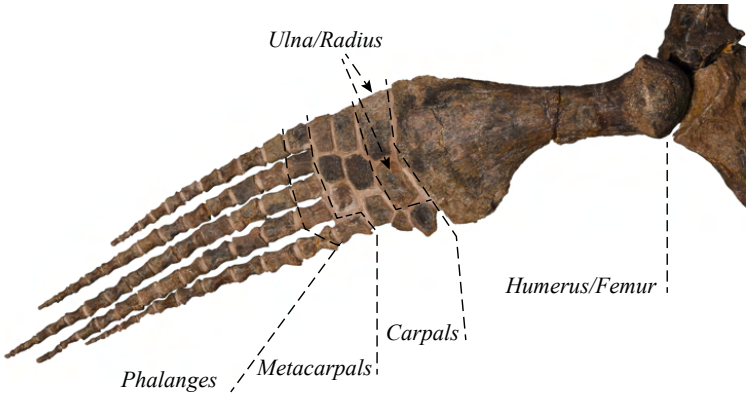

Figure 1.2: Fore flipper components of *Trinacomerum osbornii*. Courtesy of Dr. Donald Henderson.

pectoral (shoulder) and pelvic (hip) girdles (see Figure 1.2). These sockets are called glenoid and acetabulum, respectively. The rounded, almost hemispherical head of the propodials (humeri/femurs) have a smooth articular surface, and then it roughens at the perimeter and the texture changes to a striated one on the external surface of the bone. In life, there would have been a cartilage cap on this region, which would have filled the gap between the bone. The hemispherical head of the humeri/femurs will be used to estimate the dorsoventral motion range of the flippers in Chapter 2. The roughened perimeter bone texture marks the limit of the cartilage cap. In life, the animal would not have moved its flippers to the full angular extent seen on the bone. The cartilage, muscles and other connective tissue would have acted to limit the range of angular excursion. Estimating the amount of the cartilage is not easy. However, it could have been approximated by measuring the gap between the sockets and the propodials, or by measuring the cartilage limitation effect on the extant animals which have close resemblance to plesiosaur limb morphology (Carpenter et al., 2010). The latter approach is tested on sea turtles in Chapter 2.

Plesiosaur flippers are connected to the rest of the body via pectoral (shoulder) and pelvic (hip) girdles. Pectoral girdle mainly consists of scapula and coracoid, which are anterior and posterior components of the girdle, respectively. These two elements pair together to form a cavity, or glenoid as mentioned in the previous paragraph, to accommodate the humerus as seen in Figure 1.3. The elements of pelvic girdle are pubis, ischium and ilium, which are the anterior, posterior and dorsal components, respectively. Together they form a cavity (acetabulum) accommodating femur. Ilium is attached to ischium and connects the pectoral girdle to sacral ribs.

The fore and hind flippers are geometrically identical and are very similar in size, unlike any other extinct and extant animal. However, the morphology of the fore and hind flippers was slightly different. For example, humerus and femur in long-necked plesiosaurs (plesiosauroids) are roughly similar, but the femur is often a bit smaller (O'Keefe and Carrano, 2005), more slender, and does not show a prominent muscle scar on the underside that the humerus shows. The slenderness of the femur shows that its resistance to bending is less than that of the humerus, and this corresponds to the lack of a prominent muscles scar – the femur experienced less forceful muscle contractions. The dorsoventral range of motion, which is thought to be the main motion type in plesiosaur locomotion (See next section), measured from round tip of humerus is higher than the ones measured from femur.

On the other hand, short-necked plesiosaurs (pliosauroids) had more robust hind flippers and the femur displayed a higher dorsoventral range of motion. This type of differences is also apparent between the pectoral and pelvic girdles in the specimens. Plesiosauroids, had relatively larger and more developed pectoral girdle (O'Keefe, 2002; O'Keefe and Carrano, 2005) and display evidence for large muscle origination and chest and inserting to humerus. An opposite situation is evident in pliosauroids. However, these observations do not apply for all plesiosauroid and pliosauroid specimens as they have been around for 140 million years and could have evolved variety of propulsive strategies. O'Keefe and Carrano (2005), observed that the differences between the locomotor proportions are most pronounced for large-sized animals. Through scaling analysis, they hypothesized that the effect of size might have forced them to evolve either of the extreme locomotor morphologies as seen in terrestrial mammals

1.1.2 Mode of Locomotion

Plesiosaur locomotion has been questioned from two perspectives. There has been debates on the kinematics of each flipper, as well as the relative motion between the fore and hind flippers since their discovery. The second subject is regarded as so-called "four wing problem" in the literature (Frey and Riess, 1982). These debates are subjects of the following sections.

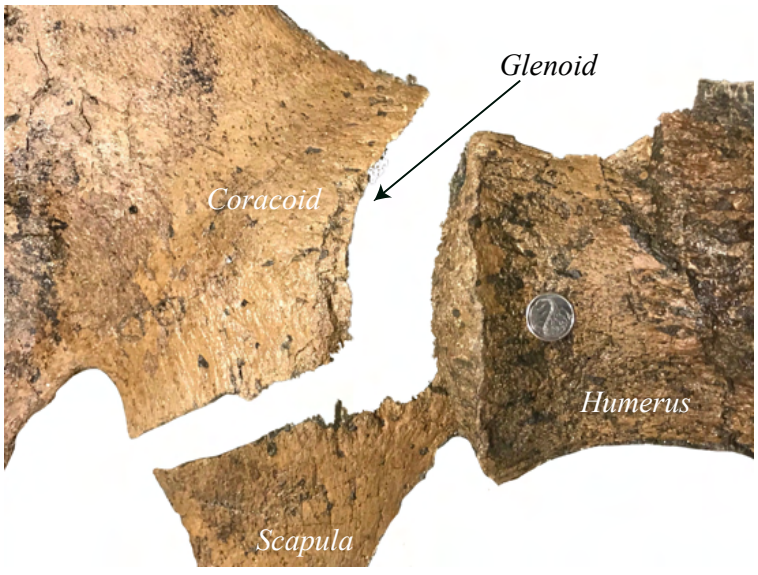

Figure 1.3: Pectoral girdle of *Wapuskanectes*. Courtesy of Dr. Donald Henderson

Individual Flipper Motion

Generally, there are three hypothesis regarding the stroke type of the flippers in plesiosaurs: rowing (anteroposterior motion), underwater flight (dorsoventral motion), and combination of both. In the rowing locomotion, which is a drag-based propulsion, animals need to extend their flippers anteroposteriorly as far as they could to push them against the water to propel themselves (Watson, 1924). This hypothesis has not received much support in the literature. However, it was put forward again recently based on a work on muscle reconstruction by Araújo and Correia (2015). Combination of rowing and underwater flight, rowing-flight, which is seen in sea lion propulsion, was suggested by Godfrey (1984). Liu et al. (2015) performed numerical simulation on plesiosaur locomotion and suggested that rowing-flight could have been possible if they flapped their flippers to maximum excursion angles.

Meanwhile, underwater flight is a lift-based propulsion, which is utilized by the vast majority of natural flyers and swimmers ranging from insects to large marine mammals. In underwater flight, as the flipper or wing moves dorsoventrally (heaving) or rotates along an axis (pitching) in fluid, due to pressure differences generated between the high pressure and suction side of the flipper, a lift force is generated. Tilting the lift force into the direction of motion results in a thrust. In section 1.2.2 this mechanism will be explained in detail. This stroke type was first suggested for plesiosaurs by Robinson (1975), due to the hydrofoil-shaped, distally tapered and flattened, and proximally cambered flippers. Later Muscutt et al. (2017b) observed that Eppler E837 hydrofoil cross-section would be the best fit for the specimen they studied.

Many animals, including sea turtles and penguins as an extant analogs of plesiosaurs, which have hydrofoil-shaped flippers, utilize underwater flight for propulsion. Recently, Krahl and Witzel (2021), were able to identify the muscles necessary for underwater flight, flipper rotation and twisting via muscle reconstruction. Storrs (1993) elaborated that the form of the glenoid and acetabulum enables dorsoventral motion and restricts protraction and retraction (anteroposterior motion). Based on the large, pitted attachment site of the ventral and posterior muscles, Robinson (1975, 1977); Muscutt (2017) argued that plesiosaurs probably had a powerful down stroke. Muscutt (2017) suggested that Godfrey (1984) rowing-flight model requires more anteroposterior motion than dorsoventral. Although rowing was possible for plesiosaurs, it might have been used for maneuverability rather than cruising as

it is inefficient drag-based propulsion. Furthermore, animals such as otters utilizing rowing locomotion, exhibit distally widened flippers Muscutt (2017). For cruising specialist such as plesiosaurs, it is very likely that they performed underwater flight as it is efficient and suitable for long-distance traveling (Walker and Westneat, 2000).

Relative Motion of the Flippers

The unique property of the close planform similarity between the fore and hind flippers, despite the different morphology, generally known as "four wing problem", has resulted in contradicting hypotheses on their locomotion. In particular, the role of hind flipper has been subject to much debate. Frey and Riess (1982) suggested that in order to avoid the vortices shed from the fore flippers, hind flippers would have moved alternatingly to ensure continuous propulsion, meaning the oscillatory motion phase lag between the flippers was $\phi = \pi$. Carpenter et al. (2010) using tandem human swimmers with plesiosaur flippers attached to their arms, concluded that plesiosaurs would have moved both flippers up and down simultaneously ($\phi = 0$), as the swimmers felt this was the easiest swimming method. Newman and Tarlo (1967) suggested a phase lag of $\phi = \pi/2$ and $\phi = 3\pi/2$, leading to porpoising motion (Muscutt, 2017). Liu et al. (2015) numerically simulating the plesiosaur acceleration from rest, suggested that fore flippers were dominant in propulsion.

More recently Muscutt et al. (2017b), inspired by tandem flapping foil studies, experimentally showed that in the cruising condition, hind flippers would have experienced 60% higher thrust generation and 40% higher efficiency if they flapped in harmony at an ideal phase lag between the fore and hind flippers. In these experiments they used realistic tandem plesiosaur flippers undergoing dorsoventral flapping motion (heaving and pitching) moving to the maximum excursion range measured from fossils. The flapping frequency and forward speed was set to match an efficient cruising mode obtained based on the evolutionary scaling constants, which will be elaborated in the next section. In their experiments, they considered different inter-flipper spacings to represent most of the plesiosaur specimens, however, both flippers flapped at the same excursion range. They concluded that propulsive performance of the hind flippers primarily depends on the phase lag and spacing between the fore and hind flippers, suggesting that different plesiosaurs would have had different propulsion strategies.

The work by Muscutt et al. (2017b) is the most advanced study on plesiosaur locomotion to date, which considered a broad parameter space. However, none of the aforementioned

works considered the differences observed in the size and development level of the fore and hind flipper morphologies. These differences could have resulted in different excursion ranges between the flippers of a specimen, and subsequently, different swimming strategies, which is one of the objectives of this thesis to study.

Implications of Neck Length

Some of the plesiosaur specimens had extremely long necks. Among them, Elasmosaurids exhibited very long neck lengths up to 7 m long, which is 63% of the total body length (Kubo et al., 2012). Therefore, it might sound impractical to fully comprehend plesiosaur locomotion without studying the effect of neck length. However, in a recent study Troelsen et al. (2019), using numerical simulations, showed that in forward swimming, elongated neck did not noticeably increase the drag force. Although they found that specimens with thicker necks probably had experienced lower drag compared to thinner ones. As the effect of neck length seems to be negligible in cruising forward locomotion, it will not be any further discussed or investigated in the present thesis.

1.2 Flapping Foils

In the previous section, based on the evidence from fossil records and hydrofoil-like planform of the flippers, it was determined that plesiosaurs might have utilized underwater flight for cruising, which is employed by a broad range of extant natural flyers and swimmers. This type of locomotion, often known as lift-based or flapping propulsion, can be abstracted by oscillating foils (Anderson et al., 1998; Lucas et al., 2020). In this section, the aerodynamic/hydrodynamic background knowledge related to oscillating foils will be covered briefly in order to understand the flapping propulsion of plesiosaurs.

1.2.1 Characterizing Parameters of Flapping Propulsion

As in many other areas of fluid mechanics, non-dimensional numbers play an important role in characterizing the oscillatory motion of the flapping foils and their relative flow field. The most important dimensional parameters associated with flapping propulsion in cruising mode are stroke amplitude, frequency of oscillation, and freestream velocity, and most non-dimesnional parameters are constructed from these. These parameters are generally

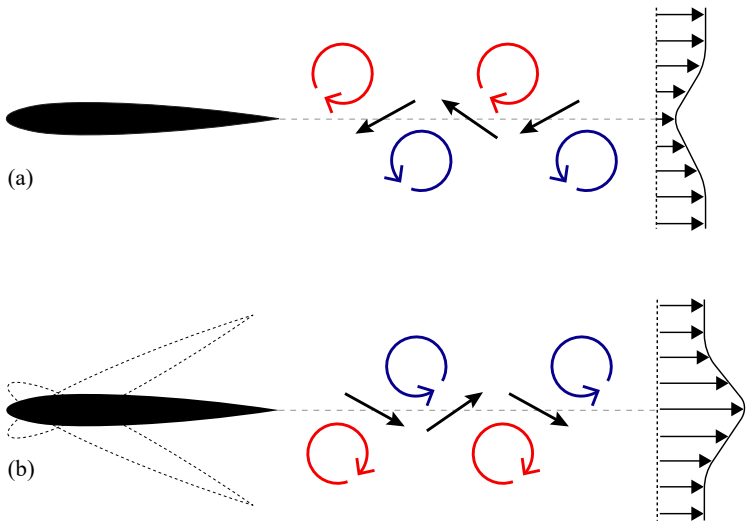

Figure 1.4: Comparison of vortical structures in the wake of: (a) stationary foil, and (b) pitching foil at relatively high Strouhal number.

discussed in terms of non-dimensional numbers, which enable comparing flapping systems of different sizes and scales, and further characterize the physics associated with the flow field of flapping foils.

The oscillatory motion of a foil can be described in terms of Strouhal number,

$$St = \frac{2Af}{U_\infty}, \tag{1.1}$$

where A denotes amplitude, f is frequency, and U_∞ is free stream or forward velocity. The Strouhal number is typically described as measurement of flapping amplitude (or wake width) and is related to force generation (Baik et al., 2012). At low Strouhal numbers a drag producing wake forms behind a flapping foil, similar to that of seen in the wake of a bluff body or stationary airfoil (See Figure 1.4a). At relatively high Strouhal numbers, the direction and position of the vortices about the center of the wake of oscillating foil reverses (Figure 1.4b), thus the vortex street transitions to thrust producing, forming so-called reverse Bénard-Von Kármán vortex street (Von Karman and Burgers, 1943). Similar figures can be found at Cebeci et al. (2005). Koochesfahani (1989) later confirmed that the velocity surplus exists in the wake of a thrust producing foil.

Triantafyllou et al. (1991), conducting experiments on oscillating foils, observed that optimal efficiency falls within the range of $0.25 < St < 0.35$. Later, Taylor et al. (2003), displayed that wide range of natural flyers and swimmers, such as insects, bats, birds, fish and marine

mammals, flap their wings and flippers within the same narrow range of $0.2 < St < 0.4$ in cruising conditions. This range happened to coincide with the optimal vortex formation, $\hat{T} = 1/St = 4$ (Dabiri, 2009), indicating that flapping at this frequency corresponds with the maximum quantity of mass that a vortex can accommodate before formation of secondary vortical structure Gharib et al. (1998), which are detrimental for the propulsive performance. $\hat{T}$ denotes the time scale of vortex formation. The evolutionary convergence of Strouhal number for cruising conditions can be extremely helpful in studying plesiosaur locomotion, as it may eliminate the need for estimating dimensional flapping frequency and swimming speed when replicating their cruising locomotion in experiments or numerical simulations, if the experiments are constructed appropriately. To investigate the reason for the maximized efficiency within the aforementioned range of Strouhal number, Floryan et al. (2018), developing a scaling model on a pitching and heaving foil, argued that the peak efficiency is highly dependent on fluid drag. The drag force itself is dependent on the Reynolds number,

$$Re = \frac{U_\infty c}{v}, \tag{1.2}$$

which is the ratio of inertial to viscous forces. Here, c denote chord length, and v is kinematic viscosity. Conducting scaling analysis, they concluded that as the result of increment of Reynolds number, offset drag decreases, subsequently resulting in increased efficiency. Here offset drag is defined as fixed body drag with the projected frontal area of the oscillating foil.

Later, Senturk and Smits (2019), showed that the model developed by Floryan et al. (2018) is a perfect representation of NACA 0012 airfoil undergoing pure pitching motion, implying that the main flow features for pitching and heaving foils are also observed for pure pitching foils.

Another important similarity parameter to describe oscillating foils is non-dimensional frequency, or reduced frequency Birnbaum (1924),

$$k = \frac{\pi f c}{U_\infty}. \tag{1.3}$$

This parameter characterizes the unsteadiness in the flow imposed due to the oscillation of the foil as it can be interpreted as the time scale of oscillatory motion to forward swimming,

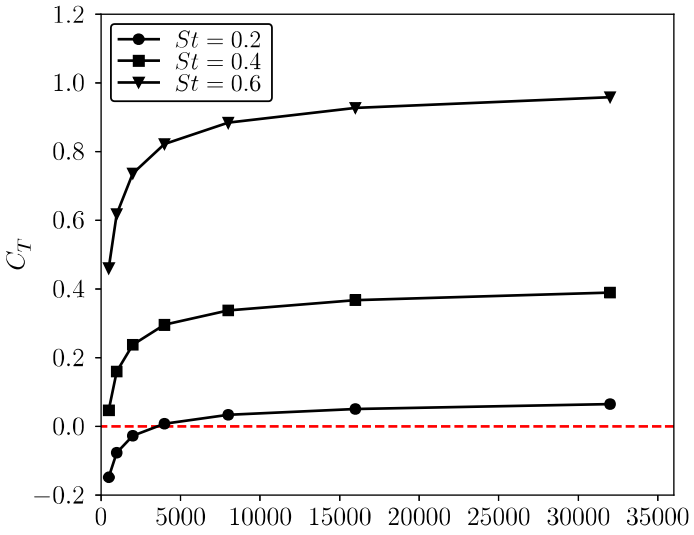

Figure 1.5: Time-averaged thrust coefficient for NACA 0012 foil pitching at $\theta = 8°$ as function of Reynolds number for various Strouhal numbers. Taken from (Senturk and Smits, 2019)

and unlike Strouhal number, it does not converge to a specific value. However, the relative maneuverability level of a flapping specimen, including plesiosaur, may be estimated based on the reduced frequency as similarity parameter, which is addressed in Chapter 2 in details as one of the objectives of the current thesis.

Floryan et al. (2018) conducting scaling analysis, demonstrated that thrust, power, and efficiency of a heaving and pitching (flapping) foil primarily depends on the Strouhal number and reduced frequency. Using numerical simulations, Senturk and Smits (2019), developed scaling relations to study the effect of Reynolds number on the performance parameters of NACA 0012 pitching foils. They demonstrated that while thrust and power coefficients scale with St^2 and kSt^2, respectively, they show relatively less sensitivity to Reynolds number scaling with $Re^{-1/2}$ as seen in Figure 5.

1.2.2 Thrust Generation

Studies on thrust generation by flapping foils begin with the investigations of Knoller and Verein (1909) and Betz (1912). They were the first to elaborate that the oscillatory motion the foil induces a velocity seen by the foil (U_{eff} in the Figure 1.6), which is at an angle with respect to the free stream velocity, known as effective angle of attack (α_{eff}). It was concluded that effective angle of attack causes the generation of resultant aerodynamic force

on the foil (N), which can be decomposed into lift (L) and thrust (T). This phenomenon is known as Knoller-Betz effect (Katzmayr, 1922).

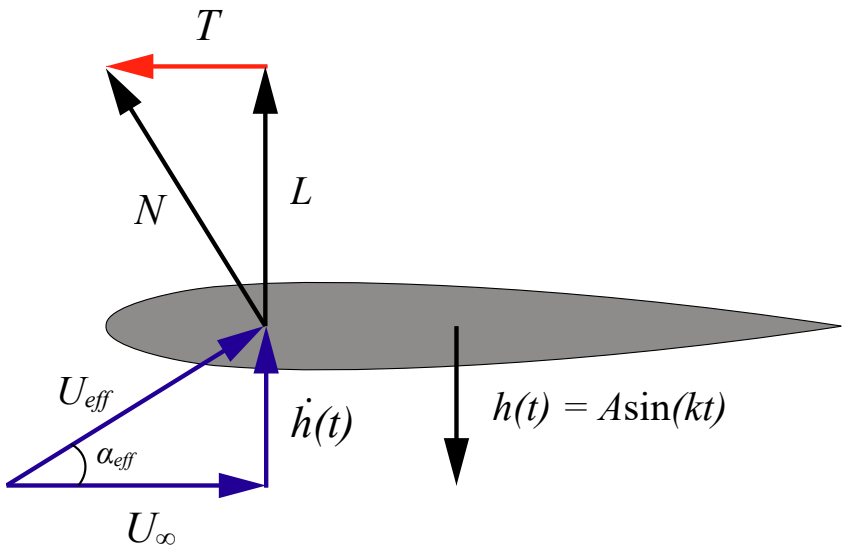

Figure 1.6: Aerodynamic forces on a heaving foil at an instant in downstroke. Redrawn from (Katzmayr, 1922).

Thrust generation of a flapping foil also can be investigated by analyzing its instantaneous vorticity and velocity fields. Due to the oscillatory motion of the foil (pitching, heaving, or combination of both), the effective angle of attack (α_{eff}) of the flow seen by the foil changes continuously. As the result of the adverse pressure gradient, if the rate and magnitude of oscillation are high enough, the shear layer at the leading edge of the foil detaches, forming the leading edge vortex (LEV) (Akhtar et al., 2007; Broering et al., 2012; Li et al., 2020). While the foil continues its motion to the end of the stroke, the LEV remains attached and results in an enhanced low pressure region at the leading edge, which subsequently results in a lift and thrust increment (Hartloper et al., 2013), which is generally known as dynamic stall. Depending on the foil kinematics, the formed LEV either sheds into the wake or becomes annihilated as a result of interaction with the foil or other shed vortices. In the latter case, at relatively high Strouhal numbers, the trailing edge vortex will shed alone into the wake, forming a very similar thrust producing wake pattern behind the foil as seen in Figure 4b. Various wake pattern can be observed behind a flapping foil depending on the foil kinematics, which is well reviewed by Anderson et al. (1998).

1.2.3 Tandem Flapping Foils

Similar to the single flapping foil case, the motivation to study tandem flapping foils arise from the observations in nature. Like plesiosaurs, dragonfly flight has received much attention due to their high maneuverability and likewise exhibiting tandem flapping wings (Rival et al., 2011; Broering et al., 2012) even though at a much smaller inter-foil spacing compared to the prehistoric example. Bird flocking Lissaman and Shollenberger (1970); Hummel (1983) and fish schooling (Weihs, 1973; Weihs and TYT, 1975; Gungor et al., 2021) are other examples that have gained much attention in recent years to prevailing role of aerodynamic/hydrodynamic efficiency in such biological behavior. In this section some of the key findings in the area of in-line tandem propulsion are briefly reviewed. More detailed review can be found in the introduction section of Chapter 3.

In-line tandem oscillating foils is a configuration of tandem propulsors in which one of the foils is positioned at the downstream of the other one and can oscillate with a phase lag (ϕ) with respect to the upstream foil. While the upstream foil is subject to free stream velocity only, the downstream foil interacts with the vortical structures shed as the result of the oscillation of the upstream foil. Generally, the interactions of the downstream foil (or foils) with these vortical structures determines the propulsive performance of the whole system, which are mainly classified as constructive or destructive interactions. In constructive cases, the cumulative performance of the system is higher than the sum of two isolated foils, where the opposite is observed for the destructive cases.

There have been many attempts to identify the characterizing parameters of thrust generation in tandem propulsion (Wu et al., 2020). One of the key studies in this area has been conducted by Boschitsch et al. (2014) in which they experimentally investigated the performance of tandem foils pitching at relatively high frequencies over a full phase space $0 < \phi < 2\pi$ across the inter-foil spacings of $0.25 - 4.25c$. Here c denotes the chord length of the foil. They identified that the performance augmentation of the hind foil is primarily dependent on the phase difference and spacing between the foils. This is because both parameters adjust the timing of the arrival of the vortices shed from the upstream foil, determining the type of wake-foil interaction of the downstream foil, and hence the mechanism of thrust generation. On the other hand, they also observed that the performance of the upstream foil was not affected by the presence of downstream foil at spacings larger than

0.5c.

By comparing Figure 1.7a and b taken from Boschitsch et al. (2014) which respectively show the variation of normalized thrust and efficiency of the hind foil for phase-spacing parameter space, it can be inferred that in tandem propulsion system, maximum thrust and efficiency occur concurrently. This is very interesting, since for a single flapping foil, maximum thrust occurs at the price of higher power consumption resulting in lower efficiency.

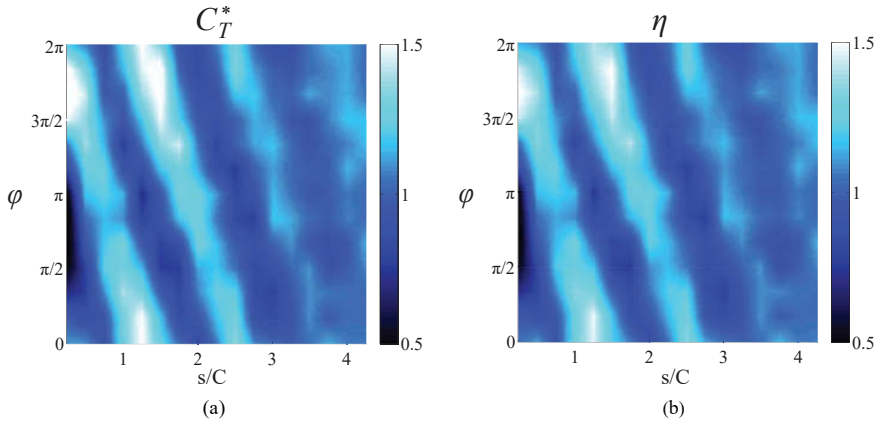

Figure 1.7: Propulsive performance results of hind foil pitching in an in-line tandem configuration. (a) Thrust coefficient, and (b) efficiency. Data are normalized by the corresponding values obtained for single foil. Taken from (Boschitsch et al., 2014).

Each of the observations above were later confirmed by studies on tandem pitching and heaving foils for a larger parameter space (Muscutt et al., 2017a; Kurt and Moored, 2018; Joshi and Mysa, 2021), confirming that similar to single foils, the fundamental flow features of tandem oscillating foils, regardless of the motion type (pure pitching, pure heaving, or combination of both), are the same.

The mechanism of thrust augmentation in tandem flapping foils is generally associated with the interaction of the vortices shed from the upstream foil with the downstream foil. In flapping foils, as described in the previous section, thrust is merely component of lift. Therefore, a constructive interaction between the vortices shed from upstream foil with the downstream foil would be the one that the pressure on the suction side, in which lift is being produced, is further decreased. Such interactions have been elaborated on in studies by Akhtar et al. (2007); Rival et al. (2011); Boschitsch et al. (2014); Muscutt et al. (2017a); Joshi and Mysa (2021) argued that at the correct phase difference, the presence of the vortex shed from the upstream foil, vortex induced velocity further increases the induced velocity

due to the foil motion, thus increasing effective angle of attack, which subsequently results in lift and thrust increment.

As discussed in the previous section, there exists a general consensus that plesiosaurs likely utilized underwater flight for propulsion. Muscutt et al. (2017b), using realistic plesiosaur flippers, conducted experiments on tandem pitching and heaving foils. The kinematics of both foils were kept identical during the experiments. Confirming the findings of previous literature, they showed that at the optimal phase difference between the foils, thrust generation and efficiency of the hind foil increases by 60% and 40%, respectively. Based on this finding, for the first time, they quantitatively showed that the hind flippers were actively involved in cruising locomotion.

Although there have been advances in understanding the swimming behavior of plesiosaurs throughout the years, none of the studies reviewed in this chapter have considered the effect of differing size and development level in morphologies. Investigating the effect of this parameter may not only help to further reveal the secrets of plesiosaur locomotion, but it might also result in defining a new optimum in tandem flapping propulsion, which is one of the objectives of this thesis.

It should be noted that biological locomotion, including plesiosaur locomotion, is a three dimensional phenomenon. One of the differences between two dimensional and three dimensional flapping foil is that in three dimensional foils, due to existence of tip vortices, the LEV formed during the oscillation may become stabilized and remain attached for slightly longer time, which generally results in higher propulsive performance (Aono et al., 2009). However, apart from tip vortices, which are secondary structures, most critical flow features of three dimensional propulsion can be inferred from a two dimensional concept such as wake-foil and vortical structures' interactions.

1.3 Contributions of the Current Thesis

Understanding the behavior and locomotion of plesiosaurs has remained as mystery primarily due to the absence of an extant analogue with the unique identical tandem flippers. In addition to this challenge, different morphologies of fore and hind flippers in a specimen have further complicated determining their swimming behavior. In order to address these challenges, two approaches have been utilized, which are detailed in Chapters 2 and 3. Each

of these chapters are under review in peer-reviewed journals.

Chapter 2 attempts to predict plesiosaur's agility level by developing a model based on universal scaling rules and evolutionary convergence observed in natural propulsion. First a model was developed to calculate the reduced frequency based on physical measurements from the animals. The proposed model then was validated across a broad range of flapping specimens from insects to marine mammals. A second validation was performed by calculating and comparing the agility level of a sea turtle using the physical information of the skeletons and kinematic information of an alive one animal. The model then was applied to plesiosaurs, providing a quantitative biomechanical analysis on the maneuverability level of plesiosaurs. For the first time, quantitatively it was confirmed that short necked plesiosaurs (pliosauroids) were more agile, like penguins, than long-necked plesiosaurs (plesiosauroids), which seem to have less maneuverability, similar to sea turtles.

Chapter 3, employs PIV measurements on tandem pitching foils to investigate the effect of the difference in size and development of the pectoral and pelvic girdles in plesiosaurs, which seem to vary from one specimen to the other. A new parameter, amplitude ratio, was defined to characterize this difference observed in the dorsoventral range of motion. It was found that plesiosaurs likely achieved to higher efficiency and thrust if they had greater hind flipper excursion amplitudes, relative to fore flippers. This is found to be more consistent with the fossil records of pliosauroids than plesiosauroids, implying that high thrust generation was easier for four-flipper motion in pliosauroids as active predators than plesiosauroids. It also conservatively implies that there might be other selective pressures than efficiency to have led to more developed pectoral girdles in plesiosauroids, or potentially two-flipper propulsion in their case. The findings in Chapter 3 also revealed that the amplitude ratio can be an important parameter to optimize the tandem flapping propulsion alongside the phase difference and inter-foil spacing.

Chapter 2

Fluid Dynamics, Scaling Laws and Plesiosaur Locomotion

2.1 Abstract

The evolutionary success of plesiosaurs has led to much attention regarding the dynamics of their locomotion. They exhibit identical tandem flippers, which is unique among all living and extinct species. However, these tandem flippers have been a source of debate regarding plesiosaurs' locomotion and behavior. Here we propose a new approach to studying plesiosaur locomotion based on universal scaling laws in fluid dynamics, which were used to estimate reduced frequency to characterize unsteadiness of an airfoil. It was found that, while the reduced frequency of plesiosaurs with high-aspect ratio flippers is similar to that of sea turtles, the most commonly used living analog, lower aspect ratio plesiosaurs were more similar in reduced frequency to penguins with higher agility. This implies that plesiosaurs may have had large variations in agility among themselves, depending in particular on the specimen's flipper aspect ratio. While our results are consistent with the previous literature indicating a relation between plesiosaur neck length and agility, with the highest aspect ratios, our work also suggests that it may be inappropriate to analogize the behavior of all plesiosaurs to sea turtles. Based on our results, cruising reduced frequency is an effective predictor of swimming behavior.

2.2 Introduction

The unique characteristic of plesiosaurs' tandem flippers, which is often referred to as the four-wing problem (Halstead, 1989; Muscutt et al., 2017b; Lingham-Soliar, 2000),has been a

source of debate on their locomotion and, therefore, their behavior (Halstead, 1989; Muscutt et al., 2017b; Carpenter et al., 2010). Apart from the study of how each of the individual flippers had moved, where the general consensus is on combination of antero-posterior and dorso-ventral motion (Muscutt et al., 2017b), contradicting hypotheses have been suggested to explain the biomechanics of why plesiosaurs had two sets of wing-like flippers while all living marine tetrapods have only one (Muscutt et al., 2017b; Liu et al., 2015). Due to the close resemblance of plesiosaur flippers to other hydrodynamic planforms such as engineered hydrofoils, one approach to the four-wing problem has come from engineering perspective (Muscutt et al., 2017b), where the assumption that the animal sought to maximize efficiency and thrust coefficients in cruising conditions was used to elucidate how the flow from both sets of flippers interacted in propulsion.

Flapping wings and flippers produce a trailing vortex wake (Wong and Rival, 2015). It has been shown that there is an upper limit for the quantity of mass that can be fed into a vortex before secondary vortices form (Gharib et al., 1998; Dabiri, 2009), known as optimal vortex formation. Those vortices formed on a wing are no different, with optimal vortex formation being described in this case with the Strouhal number (Dabiri, 2009). The Strouhal number of an oscillating wing is defined as:

$$St = \frac{2Af}{U_\infty}, \tag{2.1}$$

where f is the frequency of oscillation, A is peak-to-peak amplitude of the oscillation of the wing or flipper, and U_∞ is the forward velocity. In cruising conditions, the Strouhal number of flapping propulsion - in both air and water, from length-scales ranging from insects to whales - is observed in a limited range of $0.2 < St < 0.4$ (Taylor et al., 2003). The Strouhal number is typically described as measurement of flapping amplitude, closely associated with force generation (Baik et al., 2012). Reduced frequency, however, is a closely-related dimensionless number describing the unsteadiness of a flapping motion:

$$k = \frac{\pi f c}{U_\infty}, \tag{2.2}$$

where f is the flapping frequency, and c is chord of the wing or flipper. Reduced frequency is a ratio of time scales between flow and oscillatory wing motion. The reduced frequency can also be used to describe the time-scale on which aerodynamic or hydrodynamic forces can

change. For instance, in a study of atmospheric gusts by Wong et al. (2013), the characteristic time scale (T) of a passing gust was defined based on the time between the maximum and minimum effective angle of attack imposed on an aerodynamic surface, which was used to relate the flow velocity to the gust wavelength, $\lambda = U_\infty T = U_\infty / f$. This can be expressed equivalently in terms of the reduced frequency:

$$k = \frac{\pi c}{\lambda}, \tag{2.3}$$

where the reduced frequency here takes the form of a ratio between the length-scales of the aerodynamic surface, c, and of the gust wavelength, λ. A smaller gust wavelength (λ) represents a more rapid change of ambient conditions. This in turn means smaller time scale (T), and smaller time scale represents how quickly force can change with respect to the flow velocity or forward speed. Therefore, as an extension of this idea, reduced frequency is proposed here as a metric for agility, defined as a measure of how quickly force can change relative to forward speed.

We propose an alternative approach to study the flippers, in the context of universal scaling rules in fluid dynamics, such as convergence of Strouhal number for all flapping animals on values in the range $0.2 < St < 0.4$ for cruising conditions (Taylor et al., 2003). Using the established convergence in Strouhal number, we derive a geometric relationship between it and the reduced frequency. While the reduced frequency also characterizes unsteadiness, and may be a reasonable metric for agility, it does not exhibit the universal convergence as Strouhal number does. For example, dragonflies, known for their high maneuverability, have relatively high reduced frequencies, while sea turtles have lower reduced frequencies associated with limited maneuverability, even though they both cruise at similar Strouhal numbers. Therefore, comparisons can be made between the reduced frequency of plesiosaurs to living marine tetrapods as a means to compare their behavior. Our study introduces a new perspective to study plesiosaur locomotion by comparing its agility level to that of existing animals. We show that plesiosaurs with low aspect ratio flippers have had relatively higher unsteadiness and agility levels, while high aspect ratio ones tend to have lower agility. This implies that they have had different swimming behavior among themselves. Finally, we show that our findings of plesiosaurs agility level are consistent with previous literature studying the limits that their long necks might had imposed on their swimming behavior.

2.3 Materials and Methods

In this study, to predict plesiosaur's agility level, we follow a multistage approach. First, we propose and validate a model to predict the reduced frequency of variety of flapping appendages using only their physical layout, similar to the information available from fossil data. Following this validation, we predict a sea turtle's reduced frequency only using the data obtained from its skeleton and compare it to the actual reduced frequency calculated using the kinematics of a living sea turtle as second validation. Finally, we apply this model to plesiosaur fossils with different flipper sizes and body planforms to predict their agility level.

2.3.1 A Mathematical Method to Predict Behavior

As mentioned in the previous section, reduced frequency will be used as a metric for agility in this study. Although reduced frequency does not converge to a specific range as the Strouhal number does, some aspects of the animal behaviour can be inferred from its value. For example, insects typically have higher reduced frequencies than sea-birds, and in turn, are also associated with greater agility. However, reduced frequency is usually observed directly. Therefore, to predict the reduced frequency of an extinct species where swimming speed and flapping frequency are unknown, we must eliminate the ratio $f/U\infty$ from the expression in Equation (2.2). As this ratio also appears in Strouhal number, we can replace the ratio with a function of Strouhal number:

$$k = St\frac{\pi c}{\theta_0 b}, \tag{2.4}$$

where θ_0 (rad) is stroke angle (dorso-ventral), and b is span of the wing. The product of stroke angle and span is used as an estimate of flapping amplitude as the stroke angle, span and chord of plesiosaurs can be estimated from fossil remains. Together with the observation that the Strouhal number is approximately a constant for flapping locomotion, this reduces the cruising reduced frequency to a geometric property of the flipper and its joints. The specific value St = 0.35 is used in this study as a characteristic value, coinciding with maximum thrust coefficient and within the range of observed values in nature (Triantafyllou et al., 1991).

2.3.2 Kinematic Data

Kinematic data of 47 existing flying and swimming animals including 8 birds (Spedding, 1987; Pennycuick, 1996; Tobalske et al., 2007; Stalnov et al., 2015; Rosén et al., 2004; Henningsson et al., 2008), 12 bats (Bullen and McKenzie, 2002), 10 insects (Betts and Wootton, 1988; Rüppell, 1989; Dudley, 1990; Ennos, 1989), 3 reptiles (Davenport et al., 1984; LeBuff, 1990), 4 aquatic birds (Wilson and Liebsch, 2003; Sato et al., 2010), 9 marine mammals(Fish, 1998; Fish et al., 1988; Videler and Kamermans, 1985), and one fish (Combes and Daniel, 2001) (n=62 cases) have been collected from the open literature to calculate the Strouhal number and actual reduced frequency of each animal, as well as the predicted reduced frequency using Equations (2.1), (2.2) and (2.4), respectively (supplementary material data S1). The kinematic data used to calculate the actual and predicted reduced frequencies have been acquired from the same source for each specimen. If a range of values rather than an exact value was given for a specific parameter such as cruising speed, the average value of the provided range is used for the calculations. Where flipper chord was not measured, we calculated the chord as $c = S/b = b/AR$, where c is the chord, S is the flipper area, b is the flipper span (measured from the flipper root to the flipper tip), and AR is the aspect ratio of the flipper. If flapping amplitude was provided instead of flapping angle, we approximated the angle as $\theta_0 = 2\sin^{-1}(A/b)$, where θ_0 is flapping angle, A is flapping amplitude and b is flipper span. If data for a parameter in Equations (2.1), (2.2) and (2.4) was not reported for a specific animal in the reference literature, an additional source such as a different literature or online videos have been used to estimate an approximate value for the missing measurement, which is provided in the supplementary material data S1 as additional source. For living sea turtles, an average value for the flapping frequency and the flapping angle is used to estimate reduced frequencies. As data for these parameters were missing in the reported literature, we measured them from online videos, which the source link and measuring time is provided in the supplementary material data S2 (Table A.1 in Appendix A) as reference.

2.3.3 Sea Turtle Skeletal Measurements

To measure the flapping angle from sea turtle skeletons, Computed Tomography (CT) scans of the humerus of a *Caretta caretta*, a *Chelonia mydas* and an *Eretmochelys imbricata* were gathered from an online resource. The CT scans are provided via Harvard Museum of

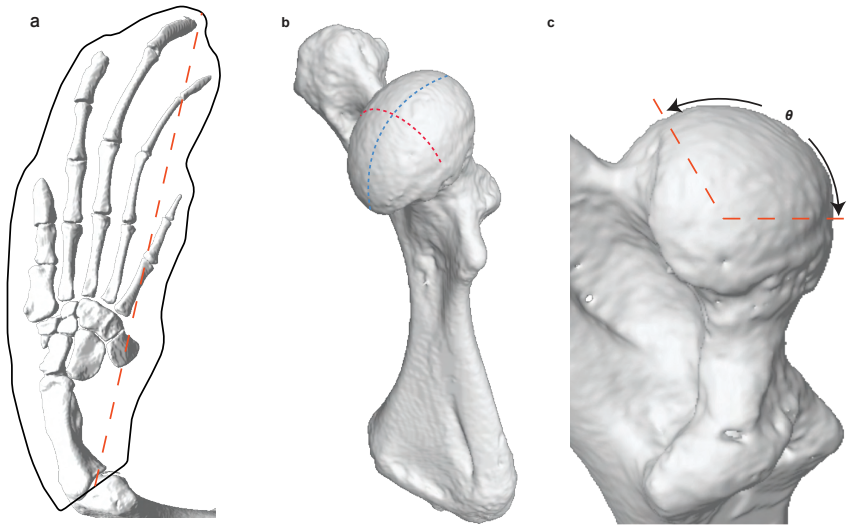

Figure 2.1: Skeletal reconstruction and measurements of *Caretta caretta*, the model organism in this study. (a) Outlining and measuring flipper area and span (the orange dashed-line). (b) demonstrating the bisector plane of the humerus head (red dashed curve) on which the flapping angle is measured. (c) Measuring the flapping angle from the angular extent of proximal end of humerus from scapulohumeral joint.

Comparative Zoology (see the supplementary material data S3 for citation and specimen numbers). A complete flipper CT scan of an adult *Caretta caretta* was gathered from Royal Veterinary College to measure both flapping angle and flipper aspect ratio (see the supplementary material data S3 for the reference (Table A.2 in Appendix A)). A three-Dimensional (3D) skeletal model is reconstructed via Object Research Systems (ORS) Dragonfly software. Skeletal measurements have been done via ImageJ software. To estimate the flipper aspect ratio as $AR = b^2/S$, the flipper area was outlined and measured as seen in Figure 2.1a. The flipper span was measured from the joint between humerus and ulna and radius (elbow joint) to the tip of the phalanges. The head of the humerus is analogous to a three-dimensional, tri-axial ellipsoid, where the flapping angle takes place about the longest axis of this ellipsoid. Flapping angles were measured from the angular extent of proximal end of humerus from scapulohumeral joint and about the longest axis (Figures 2.1(b),(c)). The plane on which flapping angle was measured is the bisector of the humerus head and the center of the rotation is the center of the angular extent of the proximal end of humerus. The measurements are presented in the supplementary material data S3 (Table A.2).

To calculate the limit that articular cartilage in the scapulohumeral joint along with the muscle traction can exert on the limb movement in dorso-ventral direction, we deducted the

average flapping angles of swimming sea turtles measured from online videos (122.13 degrees) from the average flapping angle measured directly from skeletons (136.67 degrees). Following the mentioned calculations, the cartilage limits has been estimated as 14.54 degrees in the dorso-ventral direction. Based on our measurement process, we will only continue with the first two significant digits (15 degrees) accounting for cartilage limits.

2.3.4 Plesiosaur Skeletal Measurements

To predict the reduced frequency of plesiosaurs using Equation (2.4) using kinematic data, we performed complete measurements of the aspect ratio and flapping angle of three individual plesiosaurs: *Albertonectes vanderveldei*, 'Parson's Creek' and *Trinacomerum osbornii*. For the specimens such as *Thalassomedon hanningtoni, Cryptoclidus oxoniensis*, 'Sage Creek', *Liopleurodon ferox, Nichollssaura borealis, Rhomaleosaurus thorntoni, Tatenectes laramiensis, Brancasaurus* and *Meyerosaurus* that we were unable to measure the flapping angle due to the fossil conditions, we only measured their aspect ratio. For the flapping angle of these specimens, we used an average value and a range of measured flapping angles of other specimens in the Royal Tyrell Museum to address the uncertainty range of their reduced frequency. The effect of applying this approximation is discussed in the next section. To estimate the flipper aspect ratio as $AR = b^2/S$, the flipper area has been measured in the same way as sea turtles using an internally developed script which is explained in details in (Henderson, 2003). Figure 2.2 demonstrates the fore flipper and humerus of *Albertonectes vanderveldei*. The span is determined by finding the maximum perimeter distance from the midpoint of base of the flipper (figure 2 (a)). Flapping angles were measured from the proximal end of humerus and femur (Figure 2.2 (b)). Figure S1 and Figure S2 in the supplementary material demonstrate the annotated flipper images of *Trinacomerum osbornii* and Parson's Creek, respectively (Figures A.1 and A.2 in Appendix A).

From plesiosaur remains, it can be seen that, like most flapping-like motion, both antero-posterior and dorso-ventral motions were possible for plesiosaur flippers. However, for most flapping wings and flippers observed in nature, dorso-ventral motion is the dominant motion responsible for propulsion. Therefore, we predicted reduced frequency of plesiosaur considering dorso-ventral angle. In well preserved specimens of plesiosaurs the humeral head can be seen to be almost hemispherical. There is a distinct difference in bone texture between the surface of the head of the humerus and the lateral surface of the remainder of the bone.

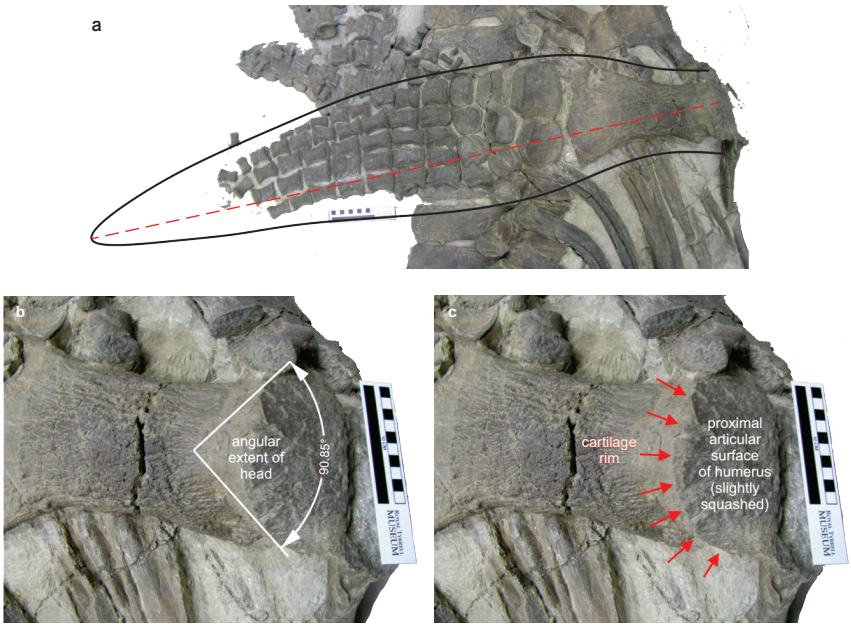

Figure 2.2: Fore flipper of *Albertonectes vanderveldei*. (a) Outlining and measuring flipper area and span (the red dashed-line). (b) Measuring the flapping angle from the angular extent of proximal end of humerus from scapulohumeral joint. (c) Demonstrating the cartilage marks on the tip of the humerus which is assumed to limit the range of the motion of the flipper.

The head is either smooth, or distinctly pitted with a texture unlike that of lateral surface. The junction of these two surfaces was taken as defining the perimeter of the head. In many cases there is also a raised rim at the junction of the two surfaces. To estimate the angular extent of the humeral head two co-terminal radii were positioned so that they tangentially contacted opposite sides of the head, and had their common origin located within the bone, but at an arbitrary distance from the head. This distance was set by the configuration of the radii and their points of tangency to the head. This measuring was either done graphically with a digital photograph in the drawing program Corel-DRAW! or done with a large protractor and two rulers on physical specimens. The true size and extent of the original soft tissue comprising the cartilage covering of the head of the humeri of the extinct plesiosaurs is unknowable. It was decided to infer conservative estimates of the flapping angles such that they would stay within the observed angular extent of head of the humerus and the selected values are compatible with the observed angular extents of the smooth-headed portions of the humeri (Figure 2.2 (c)). The measurements, specimen numbers and related references are presented in the supplementary material data S3 (Table A.3 in Appendix A) for each

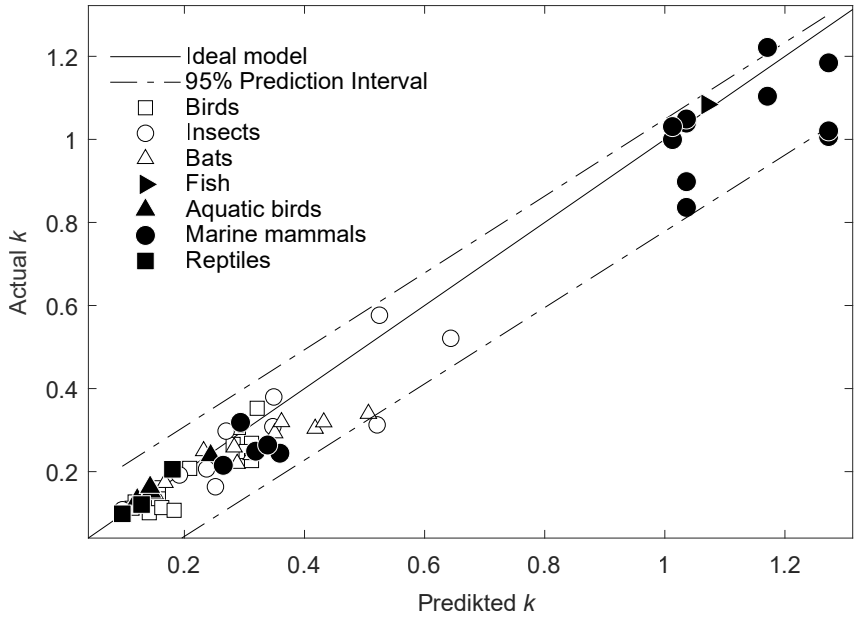

Figure 2.3: A comparison of predicted reduced frequency with and actual reduced frequency. The comparison has been made for 47 flapping species (n=62) in cruising condition within the range of $0.2 < St < 0.4$. The regression coefficient of our model is 0.92, the determination coefficient is 0.96 and the mean squared error is estimated as 0.004.

specimen.

2.4 Results and Discussion

To validate the model for reduced frequency presented in Equation (2.4), we calculated the actual reduced frequency of a wide range of 47 existing flying and swimming animals (n=62 cases) from data available in open literature, and compared these values to those predicted by Equation (2.4). The comparison between actual reduced frequency and predicted reduced frequency has been made only for animals whose Strouhal number corresponded to cruising conditions (Taylor et al., 2003) ($0.2 < St < 0.4$). This comparison is presented in Figure 2.3, and shows good agreement between our model and observed values, within the 95% prediction interval. We followed the standard procedure for all statistical analysis including regression, two-sided prediction intervals and mean squared error (Coleman and Steele, 2018) for our data collected from open literature in Figure 2.3.

Flapping angles in Figure 2.3 were determined from the behavior of living animals. In order to validate our model when data is limited to that obtained from fossil remains, a second validation was performed by applying the model to a living species, a sea turtle,

using both skeletal data, and observed behavior. Sea turtles are chosen for this validation due to their common use as a model for plesiosaurs (Carpenter et al., 2010; Liu et al., 2015). Data such as flipper area, span and flapping angle are obtained from computed tomography (CT) scans of an adult sea turtle, *Caretta carretta*, simulating skeletal remains (Figure 2.1). Flapping angles were measured from the angular extent of proximal end of humerus from scapulohumeral joint. To account for the reduction of mobility caused by cartilage or muscle traction on the dorso-ventral flapping angle, an average of observed flapping angles from living sea turtles was deducted from the average of the flapping angles measured from skeletons. It is found that the articular cartilage in the scapulohumeral joint along with the muscle traction can limit the limb movement approximately 15 degrees in dorsoventral direction. The difference between predicted reduced frequency from sea turtle skeleton and the average value of reduced frequency observed in nature is less than 4%, and it falls within the limits of prediction intervals demonstrated in Figure 2.3. This comparison shows that our proposed model is able to predict an animal's reduced frequency, thus its agility, only using the data obtained from skeletal remains.

Following the aforementioned validation, we applied our model to plesiosaur fossils to predict each specimen's reduced frequency. The results are shown in Figure 2.4. For the plesiosaurs from which we were unable to measure the flapping angle, we introduced an uncertainty range of reduced frequency as function of flapping angle, since flapping angle has a linear effect on reduced frequency as modelled here in Equation (2.4). The results of this analysis are included in Figure 2.4, where the squares denote the average value of the flapping angles measured from fossil remains of well-preserved specimens, i.e. *Albertonectes*, Parson's Creek and *Trinacomerum osbornii*. Calculated values of reduced frequency for each of the specimens presented in the supplementary material table S1 (Table A.4 in Appendix A). The uncertainty range of reduced frequency for the measured range of flapping angles was found to be sufficiently small to have no effect on our conclusions. Rather, we observe here greater variations among plesiosaurs with respect to aspect ratio than from uncertainty or variation in flapping angle.

Applying our model to plesiosaur remains, we observe that the aspect ratio has the most significant effect on reduced frequency among plesiosaurs. This can be seen when we compare the span length of *Cryptoclidus oxoniensis*, with lowest aspect ratio among all plesiosaurs, and *Tatenectes laramiensis* which has moderate aspect ratio flippers. Although

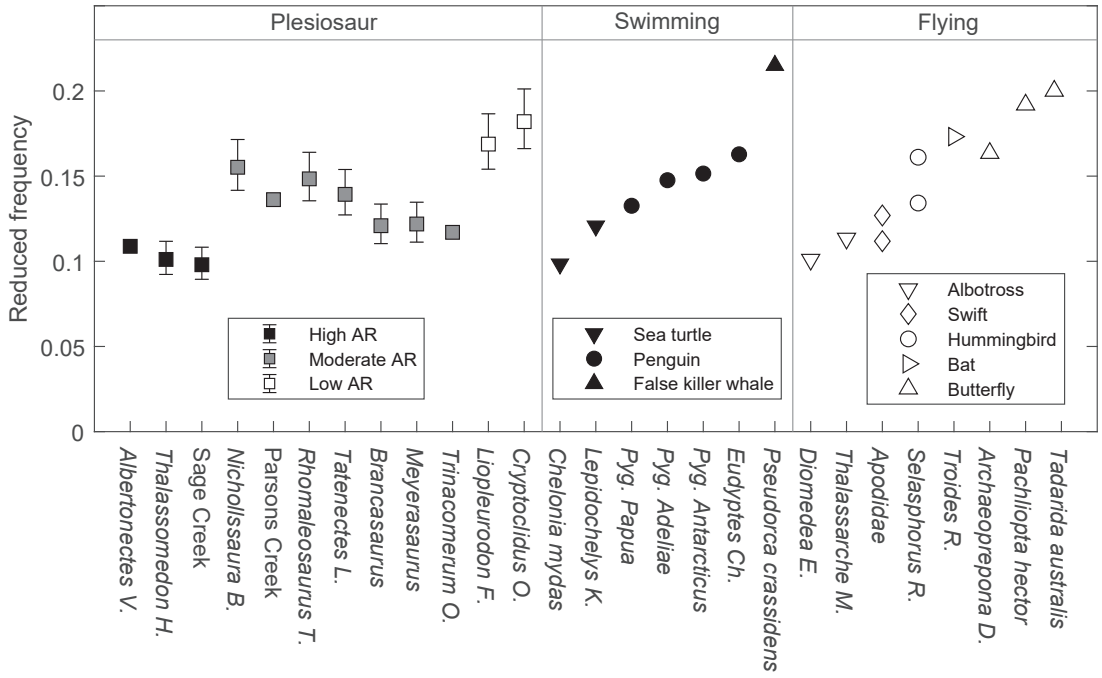

Figure 2.4: Reduced frequency of existing swimming and flying animals matching the reduced frequency of plesiosaurs. Squares on uncertainty reduced frequency bar of plesiosaurs represent the average value of reduced frequency for each group of high, moderate and low flipper aspect ratio plesiosaurs. Plesiosaur specimens might have had different level of agility among themselves depending on the flipper aspect ratio. Sea turtles are appropriate model organism only for specific subset of plesiosaurs.

they have similar span lengths, their predicted reduced frequency in Figure 2.4 reveals that *Cryptolidus oxoniensis* had significantly higher agility. Therefore, we grouped plesiosaurs into three groups based on high, moderate and low flipper aspect ratios, which correspond to low, moderate, and high reduced frequencies. Living species with similar agility to that predicted for plesiosaurs are presented in Figure 2.4. This figure also shows the reduced frequency in cruising condition gives a strong correlation with agility among living species, based on what we can observe from the behavior of animals in nature. This provides strong evidence that we can infer the level of agility of an animal from cruising-condition parameters. As seen in Figure 2.4, the *Albertonectes vanderveldei*, 'Sage Creek' and *Thalassomedon* specimens have relatively low reduced frequencies, similar to sea turtles and albatrosses. Meanwhile, *Cryptoclidus oxoniensi* with the lowest aspect ratio has the highest reduced frequency, similar to that of penguins and hummingbirds, each known for their ability to produce rapid manoeuvres. Therefore, we conclude that plesiosaurs likely had significant

variation among themselves in terms of agility and acceleration. Morphometric phylogenetic analysis conducted in previous studies also reported the possible variation in swimming techniques between different clades based on differences in girdle and limb morphology among plesiosaurs (Carpenter et al., 2010; Araújo et al., 2015). Furthermore, this finding suggests that sea turtles are unlikely to be an appropriate model organism for all plesiosaurs, and rather they are a good analog for the subset of these prehistoric marine reptiles with larger aspect ratios. Figure S3 in the supplementary material (Figure A.3 in Appendix A) shows direct comparisons between aspect ratio, flapping angle, and reduced frequency for the specimens in Figure 2.4 for additional clarity of the above observations.

Finally, we have observed that long-necked plesiosaurs consistently have high-aspect ratio flippers. In the literature, the length of the neck is understood to have an influence on agility. Plesiosaurs with longer necks are assumed to be ambush predators due to the limitations that such long necks would likely have on their ability to turn, whereas species with short or moderate necks are more likely active predators (Halstead, 1989; Massare, 1988; O'Keefe, 2002; Troelsen et al., 2019; Wintrich et al., 2019). Our findings are consistent with this hypothesis. Silhouettes of some of the specimens in Figure 42.4 are presented in Figure 2.5 to illustrate this observation. The phylogenetic tree for the plesiosaur specimens considered in this study (Benson et al., 2013), as shown in Figure 2.5, shows that the correspondence between swimming behavior and lineage is most pronounced for the long-necked specimens. Although high aspect ratio plesiosaurs with low reduced frequency are clustered around each other, low and moderate aspect ratio specimens are spread out in the cladogram, suggesting that, whereas the long neck is a significant constraint on effective behavior, a broader set of strategies are possible for the plesiosaur's flipper layout generally.

2.5 Conclusion

A new method is introduced to study plesiosaur locomotion using the universal scaling rules in fluid dynamics. In this study reduced frequency is considered as a metric to compare flapping animals' agility level as it represents how quickly force on a flipper can change with respect to the forward speed. A geometric relationship is driven between the Strouhal number and the reduced frequency using the established convergence for Strouhal number corresponding efficient cruising conditions in the nature. The proposed equation for reduced

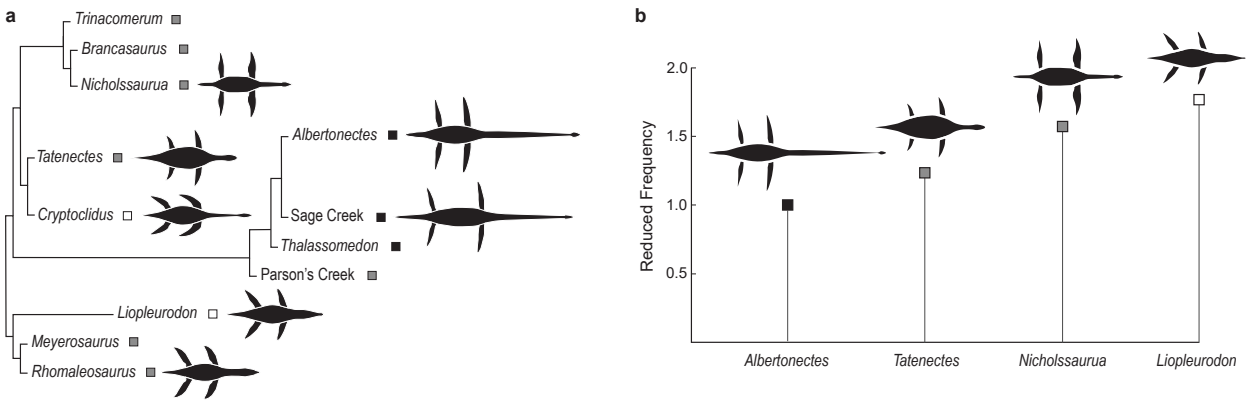

Figure 2.5: The length of the neck and plesiosaur agility. (a) Phylogenetic relationships between all groups of plesiosaurs presented in Figure 2.4. Evolution had played a minor role in determining plesiosaur behavior. The relation between neck length and flipper aspect ratio is evident from silhouettes presented in front of each specimens with different aspect ratios. (b) The effect of body planform on the reduced frequency. Plesiosaurs with shorter necks had higher agility. Silhouettes in these figures are not scaled.

frequency allowed us to predict the reduced frequency of living animals using only kinematics and geometric data. By applying the model to a sea turtle using the data obtained from both skeleton and behavior, we validated our method for the cases in which data is limited to that obtained from fossils. Following a comparison between the reduced frequency of plesiosaurs and living animals, we concluded that plesiosaurs have had different level of agility among themselves. While the reduced frequency of high aspect ratio plesiosaurs matched with sea turtles', the reduced frequency of low aspect ratio plesiosaurs matched with penguins which are more agile and maneuverable than sea turtles. This is also in consistency with the findings in previous studies considering neck length as a limiting factor for plesiosaur's agility level as high aspect ratio plesiosaurs with longer necks have lower reduced frequency and agility level comparing to low aspect ratio plesiosaurs.

Chapter 3

Constraining Optimum Swimming Strategies in Plesiosaurs: The Effect of Amplitude Ratio on Tandem Pitching Foils

3.1 Abstract

Identical tandem flippers of plesiosaurs, which are unique among all animals, have been a source of debate regarding the role of hind flippers in their locomotion. Here, inspired by the kinematics of plesiosaur flippers, the effect of amplitude ratio on the propulsive performance of in-line tandem pitching foils is investigated through a series of particle image velocimetry experiments. Three leader-to-follower amplitude ratios are considered for the foils pitching over a range of $0 - 2\pi$ phase difference. For the first time, it is shown that the amplitude ratio can significantly affect the performance of the hind foil at spacing larger than one chord length. It is found that the thrust generation of the hind foil at the optimum phase difference augments by 130% when it is pitching at the twice angular amplitude of the upstream foil. Although the total performance of the rear-biased and equal amplitude models reaches to similar values, thrust production of the hind foil in the equal amplitude model increases only by 23%. In contrast, the performance of the forward-biased model decreases drastically for all phase differences due to the destructive wake-foil interaction of the hind foil. Studying the instantaneous wake-foils interactions, it is found that high thrust generation is associated with the formation of a vortex pair on the suction side of the hind foil, which causes stronger trailing edge vortices to shed with a greater total wake spacing.

Finally, through scaling analysis, high-thrust configurations of tandem models are ranked based on the total efficiency of the system.

3.2 Introduction

Plesiosaurs, Mesozoic marine reptiles, are known for their body planform, unique among all extinct and existing animals. They exhibit identical wing-like tandem flippers, leading to controversial discussions on their locomotion, and in particular regarding the role of hind flipper in propulsion, known as "four-wing" problem (Frey and Riess, 1982). Throughout the evolution of plesiosaurs, the similarity in the size and geometry between the fore and hind flippers of the reptiles remained consistent. This is indicative of a high importance of this characteristic for plesiosaurs fitness. It was suggested that plesiosaurs with long necks and small heads were ambush predators, whereas plesiosaurs with short necks and large heads, also known as pliosaurs, were pursuit predators (Taylor, 1981; Massare, 1988). Generally, natural swimmers and flyers are capable of both impressive acceleration and maneuvering, and highly efficient cruising. These traits have led to significant interest in biological swimming and flight in the context of biomimetic and bio-inspired aero- and hydrodynamics. Many animals propel themselves by flapping their wings, flippers, or tail fins. Biologically-inspired flapping propulsion is often abstracted by oscillating foils (Anderson et al., 1998; Lucas et al., 2020). A wide range of experiments and numerical simulations have been caried out to reveal the flow dynamics and other aspects associated with the performance of oscillating foils, for instance as reviewed by Wu et al. (2020).

An early investigation of thrust generation by a flapping airfoil was provided by Knoller and Verein (1909) and Betz (1912) independently. It was discovered that the oscillatory nature of flapping motion leads to oscillatory lift, and subsequently the generation of force in the direction of flight, a phenomenon known as Knoller-Betz effect (Katzmayr, 1922). The motion of an oscillating foil can be characterized with Strouhal number, defined as $St = 2Af/U_\infty$, where A denotes amplitude, f is frequency and U_∞ is the freestream velocity. The Strouhal number is closely associated with force generation (for example, see [Baik et al. (2012)]) and may be conceptualized as the ratio of length scales of oscillation to convection. At low Strouhal numbers, a drag producing vortex street known as Bénard-Von Kármán wake forms in the wake of an oscillating foil. With increasing the Strouhal number,

the vortex street eventually inverts to become a so-called reverse Bénard-Von Kármán wake (Koochesfahani, 1989), which roughly coincides with the transition from a drag producing to a thrust producing wake (Godoy-Diana et al., 2008; Bohl and Koochesfahani, 2009). This flow pattern is very similar to that formed in the wake of natural flapping propulsors, subject to minor differences associated with flapping (rotation about a shoulder joint) versus quasi-2D oscillation (Wolfgang et al., 1999; Drucker and Lauder, 2001). Natural flyers and swimmers have been observed to flap their wings and flippers within a only a narrow range, $0.2 < St < 0.4$ in cruising conditions across a wide range of Reynolds numbers and biological origination (Triantafyllou et al., 1991; Taylor et al., 2003). This range coincides with the optimal propulsive efficiency observed in oscillating foil experiments (Anderson et al., 1998; Read et al., 2003). Experiments by Jones et al. (1998) demonstrated that the transition from thrust generation to drag production occurs in the wake of an oscillating foil when the amplitude of oscillation was increased beyond a certain critical point for fixed Strouhal number. Meanwhile, a closely-related similarity parameter is the reduced frequency, $k = \pi f c/U_\infty$ (Birnbaum, 1924), which can be interpreted as the ratio of the timescale of oscillation to the timescale of freestream convection, characterizing the degree of unsteadiness imposed by oscillation in the flow. Here, c denotes the chord length of the oscillating foil. Numerous studies have shown that while thrust increases with reduced frequency, high efficiencies are achieved at relatively low reduced frequencies (Wu et al., 2020).

For many flyers and swimmers in nature, locomotion is achieved through the interaction of multiple propulsors. For example, many fish generate thrust via complex interactions between the caudal fin and the vortices shed in the wake of the dorsal fin positioned upstream (Drucker and Lauder, 2001; Liu et al., 2017). Similarly, dragonflies adjust the phase between the fore and hind wings to switch between different flight modes (Salami et al., 2019). Akhtar et al. (2007) modeled the dorsal and tail fin interaction of bluegill sunfish via in-line pitching and heaving tandem foils. They showed that at the correct phase difference (ϕ) between the foils, the vortices shed from the upstream foil causes the leading edge vortex (LEV) on the downstream foil to stall, which in turn increases the thrust and efficiency of the downstream foil significantly. Similar wake interactions were observed by Rival et al. (2011) and Broering et al. (2012) where, inspired by dragonfly flight, they studied the effect of the phase difference between two tandem foils. Through the experiments (Rival et al., 2011) and numerical simulations (Rival et al., 2011; Broering et al., 2012) they identified two distinct

modes of either instantaneous high thrust generation, or energy extraction, depending on the phase difference. In each of the aforementioned studies, the spacing between the foils was kept constant within each study.

Other examples of tandem foil propulsion in nature include fish schooling (Weihs, 1973; Weihs and TYT, 1975; Yu et al., 2021; Gungor et al., 2021) and bird flocking (Lissaman and Shollenberger, 1970; Hummel, 1983), where favorable interactions within the flow allow neighboring animals to enhance the propulsive performance and efficiency by adjusting their flapping behavior (synchronization) and distance from the neighbor. Studies on tandem pitching foils (Boschitsch et al., 2014; Kurt and Moored, 2018) and tandem pitching and heaving foils (Broering and Lian, 2012; Muscutt et al., 2017a; Xu et al., 2017; Joshi and Mysa, 2021; Cong et al., 2020) have shown that the propulsive performance of the downstream foil is primarily determined by the phase difference and spacing of the foils. For either case, the parameters adjust the time-of-arrival of the vortices shed from the upstream foil arriving at the downstream foil. Boschitsch et al. (2014) investigated the full phase space $\phi = 0 - 2\pi$ of tandem pitching foils across spacings of 0.25-4.25c, subject to high reduced frequencies and low amplitudes. In this configuration, it was demonstrated that, at spacings larger than 0.5c, the performance of the upstream foil was not affected by the presence of downstream foil, which was later confirmed by other studies (Muscutt et al., 2017a; Xu et al., 2017). They argued that the velocity induced by vortices shed from the upstream foil could result in leading edge separation on the downstream foil, and if this separation occurred on the suction-side of that foil, as determined by the time-of-arrival, the resulting induced vortex increased lift and thrust generation by further dropping the pressure. This subsequently results in a wake mode characterized by high-momentum and coherence (Boschitsch et al., 2014). Broader parametric studies have been conducted to address more complex tandem foil interactions, to better match behavior observed in nature. Joshi and Mysa (2021) studied the effect of leader-to-follower chord ratio in the range of 0.25-1.0 for combined pitching and heaving of tandem foils across spacings of 1-10c at $k = 0.62$. They reported that maximum thrust decreases at smaller chord ratios due to the reduced energy in the wake of upstream foil. However, it was observed that efficiency remains larger at all chord ratios for high values of thrust. Kurt et al. (2021) investigated the effect of follower-to-leader amplitude ratio across the range of 1-1.48 for phase difference of $\phi = 0-2\pi$ at a fixed 0.5c spacing. They reported that the peak collective efficiency increases by 29%, where the collective thrust was

enhanced by 63-84%.

In the paleontology literature, it has been generally argued that plesiosaurs flapped their flippers dorso-ventrally to propel themselves, known as underwater flight or lift-based propulsion, similar to penguins and sea turtles (Taylor, 1981; Tarsitano and Riess, 1982; Muscutt et al., 2017b). Therefore, plesiosaur locomotion can be abstracted by tandem oscillating foils, which is a general wake-foil interaction and vortex dynamics problem. Liu et al. (2015) using inviscid flow simulations, studied the locomotion of plesiosaurs. Although they studied acceleration from rest, they concluded that plesiosaurs were reliant on the fore flippers for propulsion. More recently, Muscutt et al. (2017b), using reconstructed plesiosaur flippers, experimentally showed that in cruising conditions, the hind flipper would have reached 60% higher thrust and 40% higher efficiency if both the fore and hind flippers flapped in harmony with a particular ideal phase difference. It was argued that the general flow and vortex shedding is independent of the flipper planform, as they are also observed in two-dimensional tandem flipper simulations. In their experiments, they considered the effect of spacing (either three or seven chord lengths) and the effect of frequency (Strouhal number) on the propulsive performance of the hind foil. However, both the fore and hind foils had the identical frequency and amplitude of oscillation in each of the configurations they investigated.

Although the physical planform of plesiosaur flippers was likely identical, the morphologies of the fore and hind flippers were slightly different. Fossil records show that the fore flippers of long-necked plesiosaurs had higher angular amplitude range than hind flippers (Liu et al., 2015; Carpenter et al., 2010), and the pectoral (shoulder) girdles were more developed than pelvic girdles, unlike short-necked plesiosaurs (pliosaurs), which had more developed pelvic girdles (O'Keefe, 2002; O'Keefe and Carrano, 2005). Furthermore, assuming identical kinematics for both flippers is an ideal condition which might not be the choice of an animal in the nature for cruising condition. In this study, inspired by the difference observed in morphologies and the angular excursion range between the plesiosaur's two sets of flippers, through a set of particle image velocimetry (PIV) experiments, we attempt to understand the effect of amplitude ratio on the propulsive performance of high amplitude tandem pitching foils, and its relationship with the phase difference between the foils. Furthermore, we elaborate on the underlying mechanism of thrust generation in the studied configurations by analyzing the wake-foil interactions in detail. The results presented in the current work may be valuable to inform future studies focusing on plesiosaur locomotion or

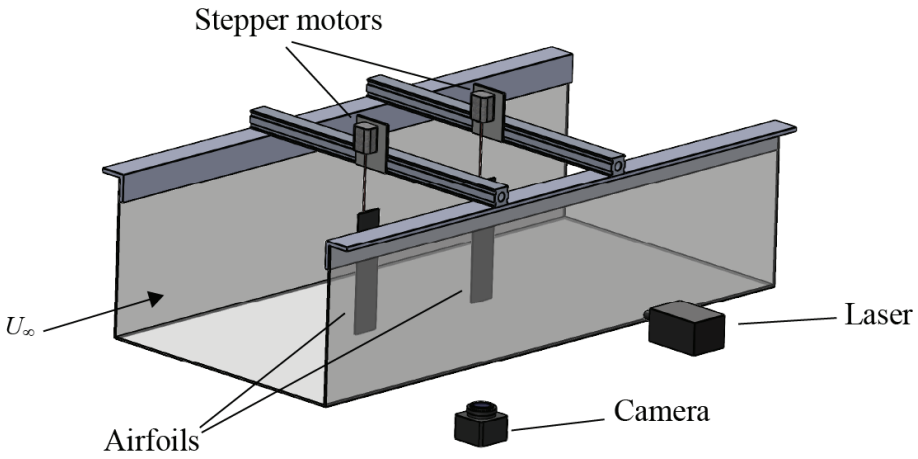

Figure 3.1: Experimental setup and PIV configuration utilized in this study. The camera captured the flow field from the underneath of the water channel, while the laser illuminated the flow field from side.

efficient marine/aerial vehicle design.

3.3 Methodology

The experiments were conducted in a recirculating open-surface water channel with a cross section of 0.68 × 0.47 m, length of 5.2 m and turbulence intensity of 4% (Hilderman, 2004). The water depth was maintained at 0.35 m throughout the experiments. Two identical airfoils with a NACA 0012 cross section and $c = 0.069$ m chord were mounted vertically from above the channel [see Fig. 3.1]. The airfoils were manufactured as continuous aluminum extrusions. To limit three dimensional effects, the gap between the foils and the floor of the water channel were maintained at 5% of chord length. The pitching axes was the aerodynamic center of either airfoil, and was driven by independent stepper motors (PK258-02Dl, Oriental Motor). Motion control was achieved by microcontroller. The fore foil was pitched harmonically at $\alpha_{\mathrm{f}} = \alpha_{0,\mathrm{f}}\sin(2\pi ft)$ while the hind foil was pitched with a phase difference (ϕ) at $\alpha_{\mathrm{h}} = \alpha_{0,\mathrm{h}}\sin(2\pi ft + \phi)$, where f is frequency, t is time, $\alpha_{0,\mathrm{f}}$ and $\alpha_{0,\mathrm{h}}$ are the maximum angle of attack of the fore and hind foils, respectively.

In this study, the amplitude ratio is defined as the ratio of the maximum angles of attack of the fore foil to the hind foil (pitch amplitudes), $Ar = \alpha_{0,\mathrm{f}}/\alpha_{0,\mathrm{h}}$. This definition is slightly different than that given Kurt et al. (2021) describing the amplitude ratio as the ratio of

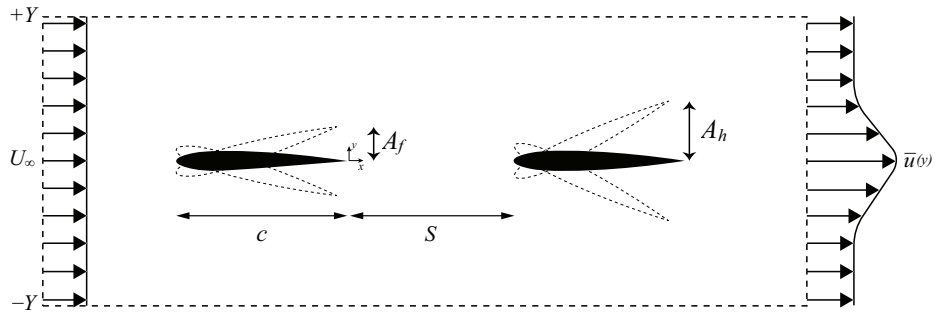

Figure 3.2: Control volume surrounding the tandem foils.

trailing edge amplitudes of the foils. However, the difference in the numerical values of Ar determined by either derivation is small for the parameters in this study, and therefore does not affect the results or the conclusion of this study. The trailing edge amplitude of the motion is obtained as $A_{\mathrm{f}} = (3c/4)\sin(\alpha_{0,\mathrm{f}})$ for the fore foil and $A_{\mathrm{h}} = (3c/4)\sin(\alpha_{0,\mathrm{h}})$ for the hind foil [Fig. 3.2]. For all measurements, in order to isolate the effect of amplitude ratio (Ar) on the propulsive performance of the tandem system, all parameters except the amplitude of the fore foil (A_{f}) and phase difference (ϕ) between the foils, are constants. Three amplitude ratios of $Ar = 0.5$, 1.0 and 1.5 (represented respectively as $Ar_{0.5}$, Ar_1 and $Ar_{1.5}$ models) were investigated in this study. For each of the tandem models, 8 phase differences ($0 < \phi < 2\pi$ with $\pi/4$ increment) were set between the foils, totaling in 24 tandem pitching configurations to study. The free stream velocity was maintained at $U_\infty = 0.078$ m/s. The frequency of oscillation was identical for both foils at $f = 0.44$ s^{-1} throughout the experiments. Therefore, the chord based Reynolds number was $Re_c = U_\infty c/v = 5382$ and the reduced frequency was $k = \pi f c/U_\infty = 1.22$, where v is the kinematic viscosity of the water. The Reynolds number is within the range used in previous studies of tandem pitching foils (Boschitsch et al., 2014; Kurt and Moored, 2018). The Strouhal number is defined based on the trailing edge amplitude of the foils as $St = 2Af/U_\infty$. As this study is inspired by plesiosaurs, the inter-foil spacing was set to $S = 3c$ to be consistent with the measurements of a recently studied specimen by Muscutt et al. (2017b). The pitching angle of the hind foils and fore foil of Ar_1 model was chosen as an average value of the dorso-ventral flapping angle of three plesiosaur specimens (67°) as reported by Muscutt (2017), and the pitch amplitude of the fore foils of $Ar_{0.5}$ and $Ar_{1.5}$ were chosen to closely represent the minimum and maximum flapping ranges measured from plesiosaur fossils, respectively (Liu et al., 2015; Muscutt, 2017). Other parameters such as freestream velocity and frequency

Table 3.1: Summary of the kinematics of fore and hind foils in each of the tandem configurations.

Model	Ar	$\alpha_{\text{max,f (deg)}}$	$\alpha_{\text{max,h (deg)}}$	St_{f}	St_{h}
$Ar_{0.5}$	0.5	16.5	33.5	0.17	0.32
Ar_{1}	1.0	33.5	33.5	0.32	0.32
$Ar_{1.5}$	1.5	50	33.5	0.45	0.32

were picked to overlap the Strouhal number range observed in nature for efficient cruising conditions, i.e., $0.2 < St < 0.4$ (Triantafyllou et al., 1991; Taylor et al., 2003). A summary of the configurations and associated kinematics are presented in Table 3.1. Although the effect of amplitude ratio is studied here with a coarse granularity, it should be noted that further decreasing the amplitude of the fore foil in order to study the effect of lower amplitude ratios would likely result in drag production by the fore foil, and such an investigation is beyond the scope of the present study.

The flow field was characterized with a PIV system composed of a Photron FASTCAM Mini WX50 high-speed camera (2048 $\times$ 2048 pixel^2 resolution, 10 μm pixel size), and a 5W continuous-wave Nd:YAG laser (λ = 532 nm). The high-speed camera was equipped with Nikon AF NIKKOR 20 mm f/2.8D lens. The flow was seeded with polymer microspheres with the diameter of 20 μm. The images were captured at 125 frames per second (fps) for single foils (fore foils) and 200 fps for hind foils. The shutter speed was set at 1/300 second during both single foil and hind foil recordings. PIV images were processed with in a commercial software package (LaVision DaVis 8.4.0). The final interrogation window with the size of 48 $\times$ 48 pixels and 50% overlap was selected to perform the vector calculations. Each of the test cases were repeated and recorded 10 times and the results were ensemble-averaged in order to obtain the final vector fields. Uncertainty of displacement in PIV measurements, which is suggested by Raffel et al. (2018) to be 0.1 pixel as sub-pixel accuracy of particle locations, corresponds to 2% and 3.2% of free stream velocity in single foils and tandem foils measurements, respectively.

Mean thrust force on the airfoils was obtained by applying the integral momentum theorem to the control volume around the airfoils as shown in Fig. 3.2. As the variation of velocity with respect to time was sinusoidal for every oscillation cycle, it can be inferred that the unsteady momentum term should be zero when cycle-averaged. Therefore, the spatial

integral of the cycle-averaged momentum flux was equivalent to the cycle-averaged of the spatial integral. To confirm that the unsteady momentum term is zero, for one case, the time average of the instantaneous thrust was calculated and compared to the thrust obtained from the time-averaged velocity field. Following this confirmation, the steady mean thrust coefficient was estimated via following equation for all cases:

$$\bar{C_T} = \frac{2}{c}\int_{-Y}^{+Y} \frac{\bar{u}(y)}{U_\infty}(\frac{\bar{u}(y)}{U_\infty} - 1)dy. \tag{3.1}$$

Here, the overbar in $\bar{u}(y)$ denotes the cycle-averaged streamwise velocity, which was performed over two cycles. The downstream control surface was $0.7c$ downstream of the trailing edge of the single foil or hind foil, respectively. In previous studies, it is well documented that the propulsive performance of the fore foil is not affected by the presence of hind foil when the inter-foil spacing is larger than one chord length ($S > 1c$) (Boschitsch et al., 2014; Muscutt et al., 2017a; Xu et al., 2017). Since the inter-foil spacing in all experiments in the present study was set to $S = 3c$, the thrust coefficient of isolated foils obtained here can be considered as the propulsive performance of the fore foils in tandem configurations ($Ar_{0.5}$, Ar_1 and $Ar_{1.5}$), if we wish to decompose the contributions to thrust.

3.4 Results and Discussion

In this section, we first study the propulsive performance and the flow field of single isolated foils, with amplitudes matching forward foils of the three cases above. Then we analyze the effect of amplitude ratio on the performance of tandem systems in terms of the flow field, wake-foil interactions, and the interactions of the wake structures of the high-performance and low-performance cases in all tandem models.

3.4.1 Propulsive Performance of Single Foils

In order to provide a baseline for comparison, we obtained the time-averaged thrust of individual foils, with pitching kinematics matching the three different kinematic cases that would be used in tandem-foil tests later. The propulsive performance of single foil measurements obtained from the wake at $x/c = 0.7$ from the trailing edge are as follows: $\bar{C}_{T,\mathrm{f},0.5} = 0.02$, $\bar{C}_{T,\mathrm{f},1} = 0.13$ and $\bar{C}_{T,\mathrm{f},1.5} = 0.54$. As it is stated in the Methodology section, these values are also representative thrust coefficients of fore foils in corresponding tandem configurations.

Therefore, the results are denoted with additional subscripts corresponding to the analogous tandem-foil kinematics, to be consistent with later sections. It can be seen that the time-averaged thrust increases by increasing the Strouhal number, which is consistent with the literature (Boschitsch et al., 2014; Kurt and Moored, 2018; Senturk and Smits, 2019).

Comparing the performance of the single foils in this study to the ones obtained by Boschitsch et al. (2014), it can be seen that isolated foils in this study produce marginally less thrust at the same Strouhal number. This was expected, and can be explained by considering the additional effect of the reduced frequency on the performance of a pitching foil. The foils in the present study are pitching at relatively high amplitudes and low reduced frequency than the ones studied by Boschitsch *etal* (Boschitsch et al., 2014). As shown by Jones et al. (1998), for a fixed Strouhal number, the propulsive performance of an oscillating foil decreases when the oscillation amplitude is increased beyond a certain limit.

The performance of the fore (single) foil of Ar_1, $\bar{C}_{T,\mathrm{f},1}$, will be used as reference to normalize the total performance obtained for the tandem systems. We chose it as reference case because the hind foil in all tandem configurations was pitching with the kinematics of the fore (single) foil of Ar_1 configuration. Hereafter, any data referred to as 'reference' will refer to an isolated foil of this amplitude. This also corresponds to the average excursion amplitude of plesiosaur flippers (67°) as discussed in the methodology section. Therefore, the normalized performance of any tandem configuration exceeding $\bar{C}^*_T > 1$ is an indication of thrust augmentation if the hind flipper was involved in plesiosaur locomotion. Values exceeding $\bar{C}^*_T > 2$ in tandem configurations, would demonstrate that tandem flippers as a system exceed the sum of its individual flippers in isolated (uncoupled) conditions and equivalent kinematics. Further analyses are provided in the next section.

3.4.2 Flow Field of Single Foils

The instantaneous normalized vorticity field and cycle-averaged velocity field over 2 cycles of the single foil is shown in Fig. 3.3 . The instantaneous vorticity field of isolated foils representing the corresponding fore foils of Ar_1 [Fig. 3.3(c) (Multimedia view)] and $Ar_{1.5}$ [Fig. 3.3(e)] show that a reverse Bénard-Von Kármán vortex street is formed where two vortices of opposite sign shed per cycle, as expected. In the case of fore foil of $Ar_{0.5}$ [Fig. 3.3(a)] two like-signed vortices are observed to shed during each stroke. Note that the shadow casted by the foil and the regions obstructed by the parallax effect from the tip of the foil

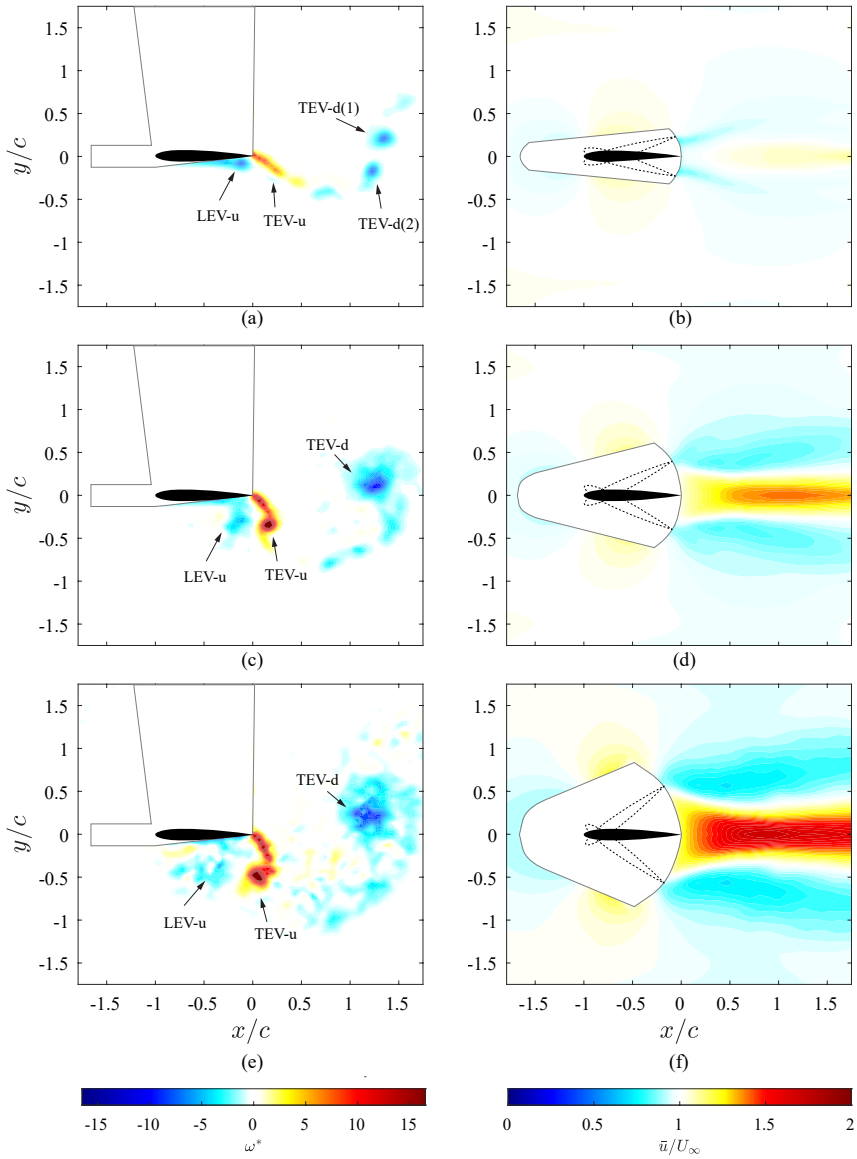

Figure 3.3: Vorticity fields (left column), and cycle-averaged velocity fields (right column) of single foils representing fore foils of: (a) and (b) $Ar_{0.5}$, (c) and (d) Ar_1, (e) and (f) $Ar_{1.5}$. Flow fields of (c) and (d) also represent the flow fields of reference single foil. Multimedia view: (c).

are covered with white polygon with grey edges. In these figures, vorticity is normalized as $\omega^* = \omega c/U_\infty$.

The vortices in the wake of the fore foil in $Ar_{1.5}$ are larger and stronger than Ar_1. In Fig. 3.3(c) (Multimedia view), focusing on the middle of the upstroke of the reference case, the leading edge vortex (LEV) forms on the lower surface of the foil during the upstroke (LEV-u) and rolls toward the trailing edge during the downstroke. Here 'u' denotes upstroke.

Once the LEV-u reaches the trailing edge at the end of the stroke, its strength decreases as it detaches and mixes with opposite-sign vorticity as the foils begins the next stoke. The weak LEV-u, after shedding, interacts with the TEV shed during the upstroke (TEV-u) and is partially annihilated. A similar interaction is seen for vortices of the single foil of $Ar_{1.5}$, except that in this case, the LEV-u detaches during the upstroke due to the very high pitching amplitude, yet remains close to the bottom surface until it reaches the trailing edge at the end of the downstroke. The time-averaged velocity filed of both fore foils of Ar_1 and $Ar_{1.5}$ [Fig. 3.3(d) and 3.3(f)] illustrate a jet wake behind the foils where the momentum of the jet is higher in $Ar_{1.5}$, consistent with the presence of stronger vortices observed in its wake. The cycle-averaged (2 cycles) flow field figures are mirrored with respect to the center of the wake to remove the shadow casted by the foil in the laser sheet. In $Ar_{0.5}$ configuration [Fig. 3.3(a)], due to its low amplitude and low reduced frequency, it can be seen that circulation from the shear layer is shed as several smaller vortices, and the two like-signed primary vortices (TEV-u1 and TEV-u2) retain their coherence as they advect downstream. The time-averaged flow field of the single foil in $Ar_{0.5}$ in Fig. 3.3(b) demonstrates a weak jet in the middle of the wake, which corresponds to the small amount of thrust produced relative to the other isolated foils.

3.4.3 Propulsive Performance of Tandem Foils

Time-averaged thrust coefficients obtained for each of the models are presented in Fig. 3.4. These thrust coefficients represent the combined tandem foil system. Thrust coefficients presented in this figure are normalized with the value obtained for the reference single foil, i.e., $\bar{C}_{T,\mathrm{f},1} = 0.13$. It should be noted, however, that the particular choice of normalization value does not affect the conclusions, as the relative performance of each case will remain the same. It can be seen that the time-averaged thrust obtained for a tandem configuration is highest for the $Ar_{0.5}$ at $\phi = 5\pi/4$. For this case, the total thrust obtained is about 2.5 times of the value obtained for the reference flapping foil, meaning the hind foil approximately achieved 130% increase in thrust than it would have in isolation. This is to say that for this particular phase difference, the small addition to the wake momentum generated by the lowest-amplitude fore foil more than doubles the thrust produced by the hind foil. Generally, it is evident that $Ar_{0.5}$ configurations produce higher thrust (or lower drag, depending on the phase difference) compared to Ar_1 and $Ar_{1.5}$ configurations. This increase in performance

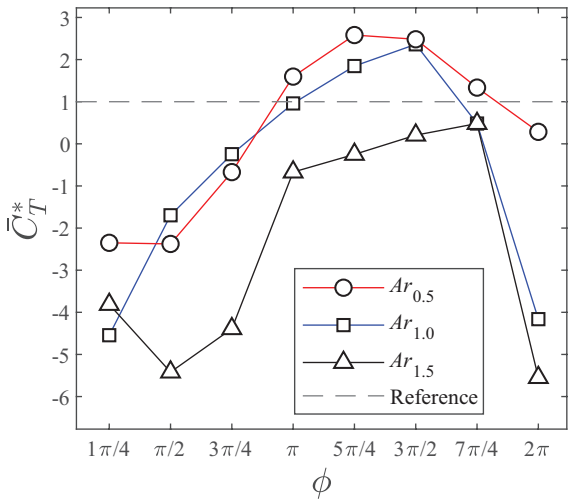

Figure 3.4: Variation of time-averaged normalized thrust coefficients of tandem configurations, $\bar{C}_T^*$, with phase difference (ϕ) between the fore and hind foils, obtained at $x/c = 0.7$ from the trailing edge of the hind foil. The dashed line indicates the normalized performance of the reference single foil.

can be explained with reference to the instantaneous flow field, which is the topic of the next section.

The highest thrust producing configuration of $Ar_{0.5}$ ($\phi = 5\pi/4$) outperformed the highest-thrust case of Ar_1 ($\phi = 3\pi/2$), but only by approximately 10%. For this phase difference, Ar_1 produced 2.2 times the thrust of the reference case, such that the thrust produced by the hind foil in this configuration was only slightly augmented (23%) by the addition of the upstream foil. This relatively small increment was expected. In addition to the effect of lower reduced frequency in our experiments, as it has been shown by Boschitsch et al. (2014), the peak thrust and efficiency are achieved at spacings $S < 2.5c$ for in-line tandem pitching foils. Our results show that $Ar_{1.5}$, when the fore foil has higher amplitude than the hind foil, produced 56% less thrust than the reference case, even at its optimum phase difference ($\phi = 7\pi/4$). All other configurations of $Ar_{1.5}$ produced either negligible thrust or drag. Presented values of thrust coefficient in Fig. 3.4 are found to be completely periodic for $Ar_{0.5}$ and Ar_1 models. Additionally, it can be seen that the optimum phase difference between the fore and hind foils increases for increasing amplitude ratio. This increment is even more evident when we compare the optimum phase difference of $Ar_{0.5}$ at $\phi = 5\pi/4$ and $Ar_{1.5}$ at $\phi = 7\pi/4$.

From the paleontological perspective, as the $Ar_{0.5}$ model, representing a rear-biased lo-

comotion, demonstrates superiority over other tandem models, it can be speculated that plesiosaurs could likely achieve higher performance by utilizing this type of locomotion. This swimming behavior is consistent with fossil records of short-necked plesiosaurs (pliosaurs), which exhibit more developed pelvic girdles than pectoral girdles. Meanwhile, fossil records of long-necked plesiosaurs exhibit relatively larger pectoral girdles, which is more consistent with forward-biased locomotion. However, as none of the configurations of $Ar_{1.5}$ model exceed the reference single foil performance, it is unlikely that they used this configuration for cruising locomotion. Another practicable model investigated in this study is Ar_1, which represents the equal-amplitude motion. Our results suggest that plesiosaurs could likely experience augmented performance by utilizing this type of locomotion, confirming the findings of Muscutt et al. (2017b). However, at the optimum phase difference, the hind foil in highest thrust phase of $Ar_{0.5}$ model achieves higher thrust than the one observed for Ar_1.

3.4.4 Flow Field of Tandem Foils

In order to understand the mechanisms causing the various amplitude ratios to produce such high and low performances, we must investigate the instantaneous dynamics of the wake structures. Following this, we present a comparative analysis between the high-thrust cases of $Ar_{0.5}$ and Ar_1 configurations to further reveal the effect of amplitude ratio on the performance of an in-line tandem pitching system.

Model $Ar_{0.5}$: In the highest thrust case, corresponding to a phase difference between the foils of $\phi = 5\pi/4$, it is seen that the two small vortices shed from the fore foil (which is pitching at half amplitude of the hind foil), denoted by TEV-uf(1) and TEV-uf(2) in Fig. 3.5(a) (Multimedia view), arrive at the vicinity of hind foil at $t/T = 0.37$ at the beginning of the upstroke. Note that t/T in Fig. 3.5 refer to time within an oscillation cycle of the fore foil and not a phase difference. Hereafter, 'f' and 'h' are used in association with 'LEV' and 'TEV' to distinguish weather the vortex is shed from the fore ('f') or hind ('h') foil. The TEV-uf(2) is weaker than TEV-uf(1) and passes far above the surface of the foil and annihilates further at the downstream not affecting the performance. The TEV-uf(1), however, arrives at the leading edge at the middle of the upstroke $t/T = 0.62$ [Fig. 3.5(b) (Multimedia view)]. This instance is concurrent with the onset of formation of LEV-uh with the opposite sign. Since TEV-uf(1) has come very close to the leading edge, it induces the leading edge. As the upstroke proceeds, the TEV-uf(1) leaves the induced LEV-uh and

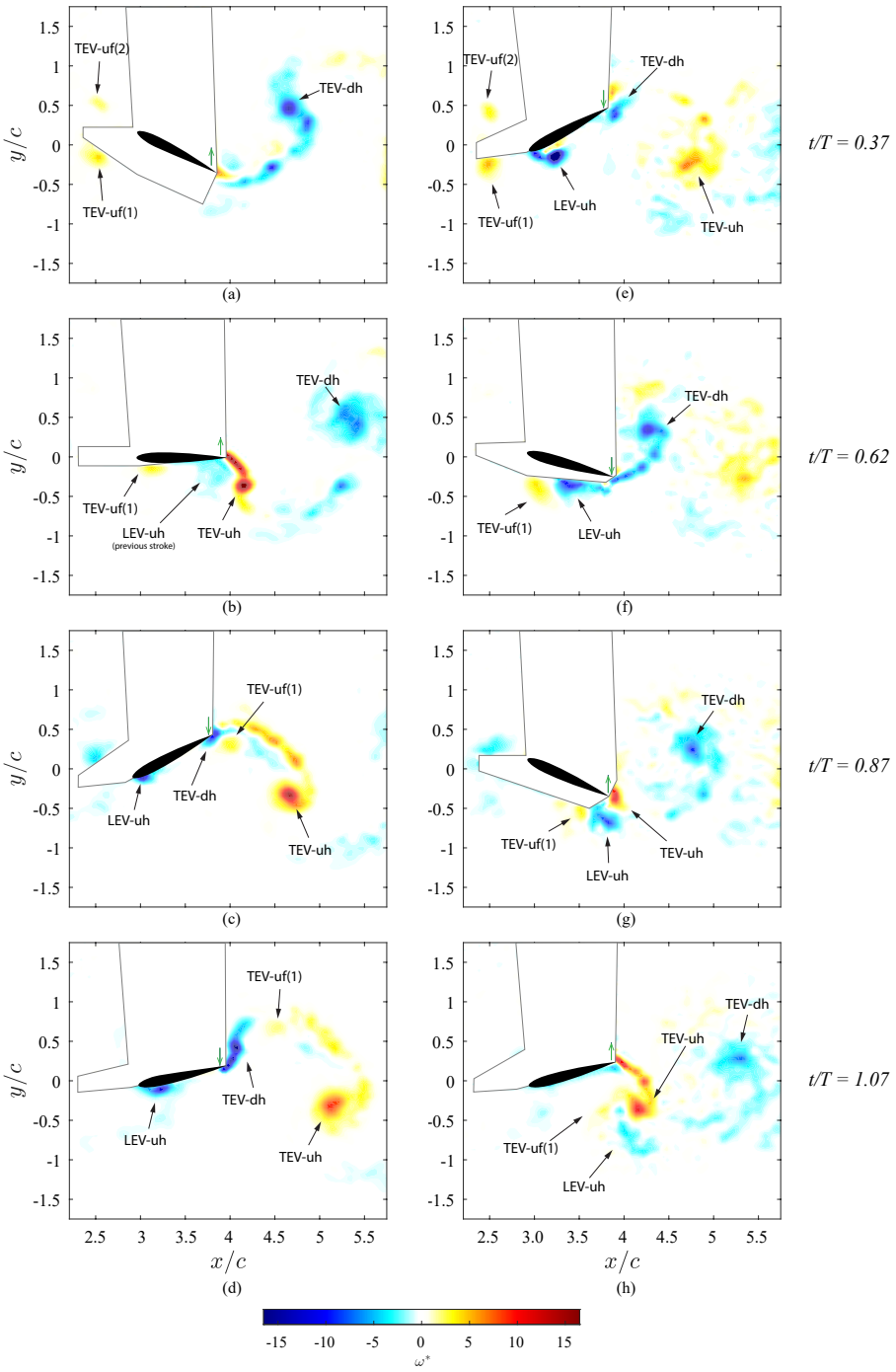

Figure 3.5: Instantaneous vorticity fields of hind foil in model $Ar_{0.5}$ at: (a) - (d) $\phi = 5\pi/4$ corresponding to high-performance case, and (e) - (h) $\phi = \pi/2$ corresponding to low-performance case. t/T denotes the time in the oscillation period of the fore foil. This figure illustrates the arrival of TEV-uf(1) at the hind foil and their interactions during one oscillation cycle of the hind foil. The green arrow positioned on the trailing edge demonstrates the instantaneous direction of the foil motion. Multimedia view: (a) - (d).

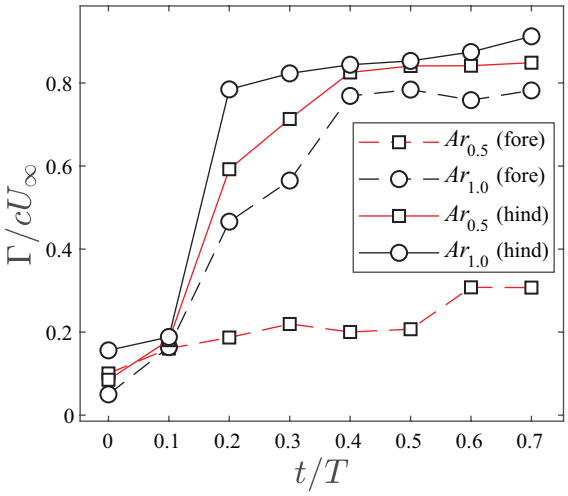

Figure 3.6: Time-history evolution of circulation of TEVs shed from the pitching foil. $Ar_{0.5}$ (fore) data represent the circulation values of TEV-df(1) in Fig. 3.3(a), and Ar_1 (hind) represent the circulation values of TEV-df+LEV-uh in Fig. 3.8(b) - 3.8(d). Note that Ar_1 (fore) data also represents the data of the reference single foil (TEV-u in Fig. 3.3c).

quickly moves toward the trailing edge while remaining attached to the lower surface of the foil due to the suction. At the end of the upstroke at $t/T = 0.87$ [Fig. 3.5(c) (Multimedia view)], the TEV-uf(1) reaches to the trailing edge inducing a larger TEV-dh which is going to be shed the next stroke i.e., downstroke. The TEV-uf(1) and the induced TEV-dh form a vortex pair which its (u_y) component of induced velocity causes the TEV-dh to shed at a farther lateral distance from the center of the wake compared to the TEVs shed from the reference foil. The TEV-dh shed from the lower surface of the foil induces the shear layer on lower surface which by the beginning of the downstroke will shed and amalgamate into the induced TEV-dh resulting in a stronger TEV than the one shed from the reference foil. This is confirmed as shown in Fig. 3.6 demonstrating the time-history of the circulation evolution of the TEVs. The circulation of the vortices is calculated along the closed contour which surrounds the vorticity. Values above 10% of the maximum vorticity were chosen to calculate the circulation. The vortex pair starts decoupling at the instance of TEV shedding and the onset of downstroke. At this instance the vortex pair decouples constructively (without generating secondary wake structures), and while the TEV-dh continues growing because of the vorticity supply from the lower surface of the foil, the TEV-uf(1) joins the like-signed secondary structures from the vorticity tail of the TEV-uh shed from previous stroke. This becomes clearer later at $t/T = 1.07$ as the downstroke proceeds [Fig. 3.5(d) (Multimedia

view)]. The LEV-uf formed at the middle of the upstroke eventually starts rolling down at the beginning of the downstroke and similar to the reference single foil becomes weaker and detached at the end of the downstroke and later gets annihilated as a result of interaction of the vortices shed from previous stroke.

The result of shedding of stronger trailing edge vortex, which is positioned at a higher lateral distance from the wake center, becomes evident in time-averaged wake shown in Fig. 3.7(a), which indicates the presence of a stronger and wider jet in the wake of the hind foil

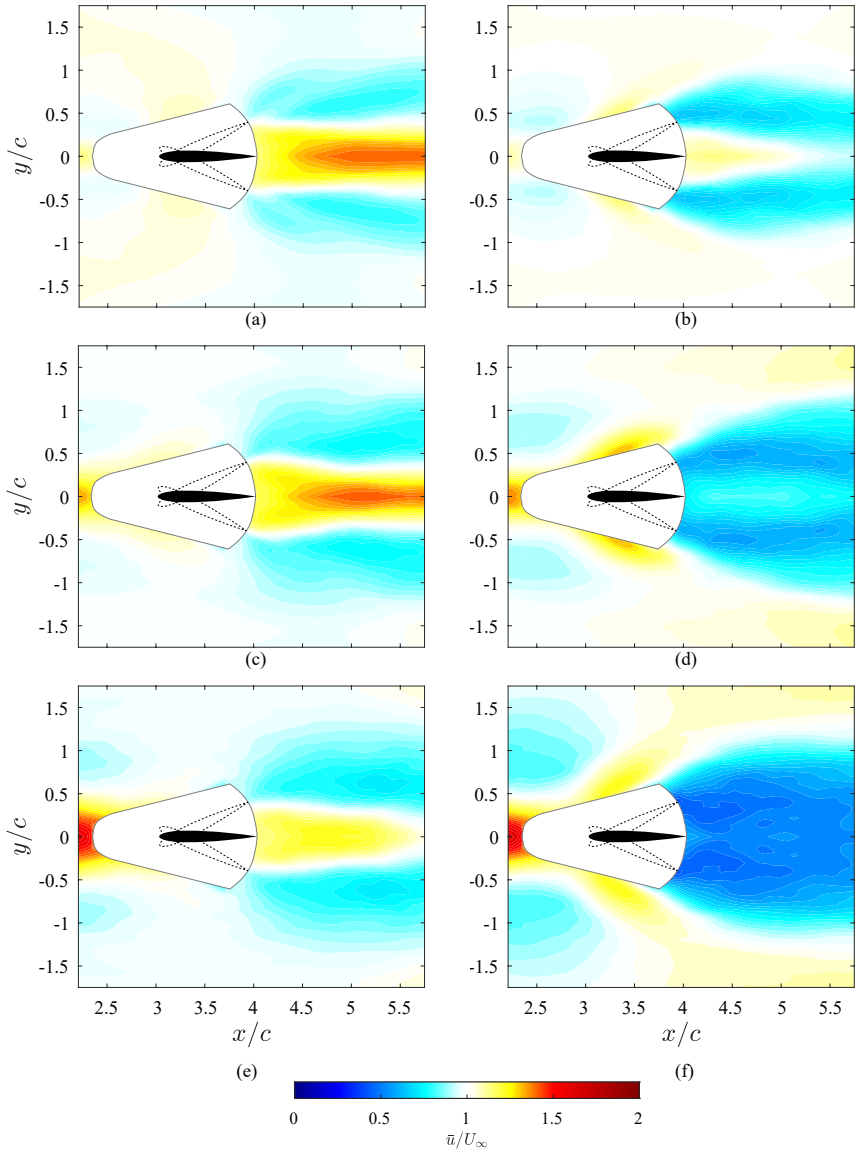

Figure 3.7: Cycle-averaged streamwise velocity field of the high-performance (left column) and low-performance (right column) of the hind foil in tandem configurations: (a) and (b) model $Ar_{0.5}$, (c) and (d) model Ar_1, and (e) and (f) model $Ar_{1.5}$.

than the reference foil. Heathcote and Gursul (2007) observed similar enhanced thrust from such wake signature, although produced through different means (flexible foils, in their case).

Conversely, when the phase difference between the foils is set to ($\phi = \pi/2$), the vortical structures of the foils did not have constructive interactions. The TEV-uf(1) arrives at the leading edge of the hind foil shortly after the middle of its downstroke at $t/T = 0.67$ [Fig. 3.5(f)]. The velocity induced by TEV-uf(1) enhances the shear-layer velocity on the hind foil, increasing the strength of LEV-dh. TEV-uf remains behind the LEV-dh until they together arrive at the trailing edge, at the end of the downstroke, where LEV-dh detaches from the trailing edge. As the upstroke begins, LEV-dh is between TEV-ud shedding from the top of the foil and TEV-uf(1) behind it, as shown in Fig. 3.5(g) at $t/T = 0.87$. This causes a reduction in circulation to LEV-dh as a result of vorticity annihilation. Eventually, as the result of this interaction and annihilation of the LEV-dh at $t/T = 1.07$, as shown in Fig. 3.5(h), smaller secondary vortices form that result in drag in the time-averaged Fig. 3.7(b).

Model Ar_1: The wake structures of the highest-thrust configuration of Ar_1 ($\phi = 3\pi/2$) is very similar to $Ar_{0.5}$ at $\phi = 5\pi/4$. In general, strong TEVs are present at the wake of the hind foil and the time-average flow field reveals a wider jet wake with higher momentum at centerline compared to the wake of the reference foil. At $t/T = 0.50$ [Fig. 3.8(a) (Multimedia view)] a single TEV-uf arrives at the leading edge of the lower surface of the hind foil, which is at that point in the middle of its upstroke. Here, the velocity induced by TEV-uf produces a shear-layer at the leading-edge, forming an LEV on the bottom surface. As the foil proceeds upstroke motion, due to the proximity of TEV-uf to the surface of the hind foil, it forms a vortex pair with LEV-uh in contrast to $Ar_{0.5}$. This vortex pair remains attached to the surface of the foil and advects towards the trailing edge as seen in Fig. 3.8(b) (Multimedia view) ($t/T = 0.60$) and reaches the trailing edge at the end of upstroke [$t/T = 0.85$ in Fig. 3.8(c) (Multimedia view)]. Similar to $Ar_{0.5}$, due to the induced velocity of the vortex pair, LEV-uh sheds farther away from the wake centerline. However, we should note the difference that in the case of Ar_1, it is the induced LEV-uh being shed, while in the case of $Ar_{0.5}$ it is the induced TEV-uh. The start of downstroke is concurrent with the decoupling of the vortex pair. In this configuration, the decoupling is not as constructive as what seen in $Ar_{0.5}$ at $\phi = 5\pi/4$ since the vortex pair is composed of stronger vortices compared to the one in $Ar_{0.5}$. As the downstroke proceeds, the shed LEV-uf induces multiple secondary TEVs on the lower surface, and the TEV-dh merges with LEV-uf, together forming a stronger

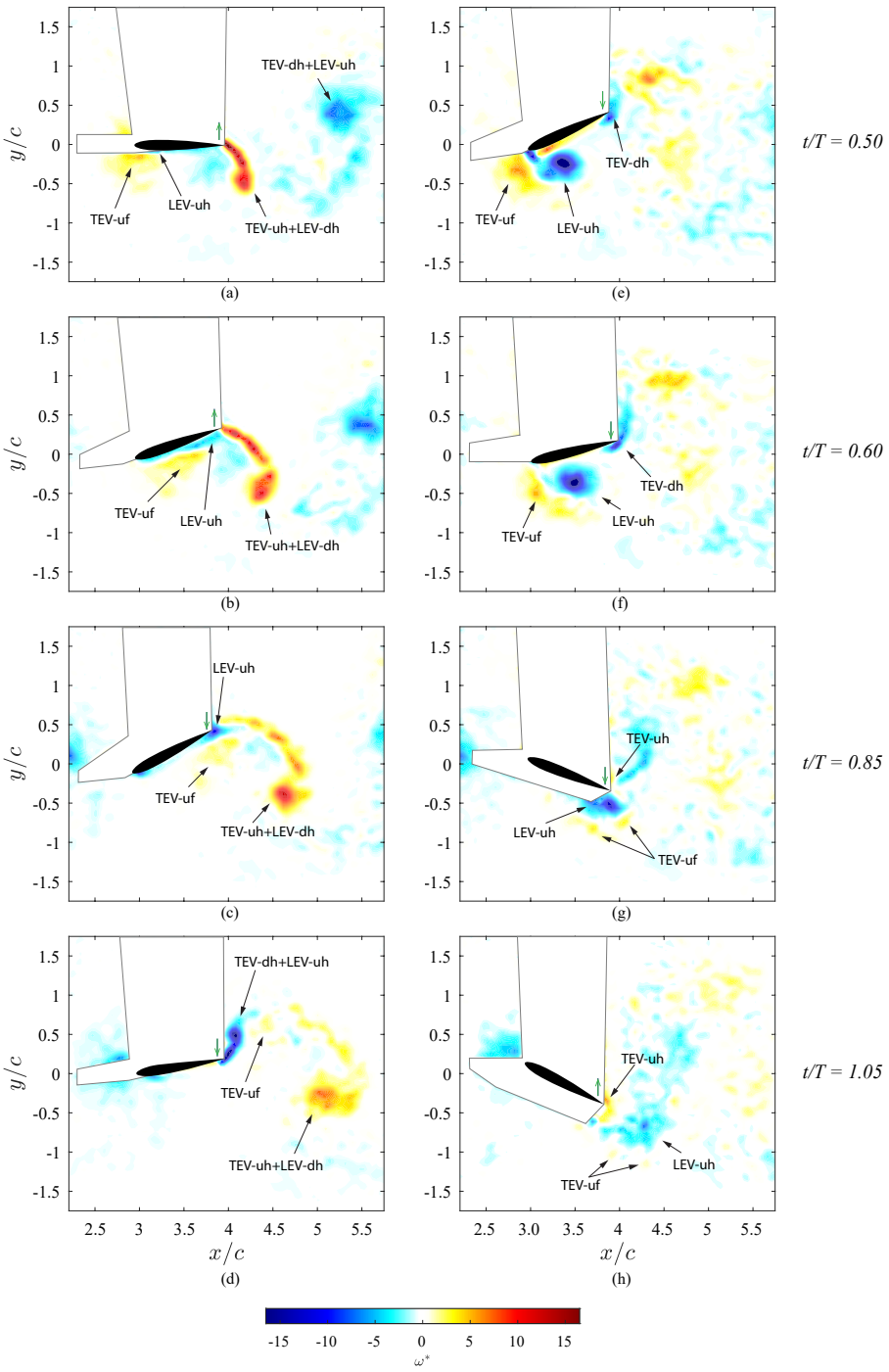

Figure 3.8: Instantaneous vorticity fields of hind foil in model Ar_1 at: (a) - (d) $\phi = 3\pi/2$ corresponding to high-performance case, and (e) - (h) $\phi = 1\pi/4$ corresponding to low-performance case. t/T denotes the time in the oscillation period of the fore foil. This figure illustrates the arrival of TEV-uf at the hind foil and their interactions during one oscillation cycle of the hind foil. The green arrow positioned on the trailing edge demonstrates the instantaneous direction of the foil motion. Multimedia view: (a) - (d).

combined vortex (denoted as TEV-dh+LEV-uh in Fig. 3.8(d) (Multimedia view)). The growth of TEV circulation shown in Fig. 3.6 indicates a faster TEV evolution in the case of Ar_1 than $Ar_{0.5}$.

The instantaneous vorticity field of the wake of the hind foil is similar to the one observed by Boschitsch et al. (2014) studying in-line tandem pitching foils, where a classic reverse Bénard-Von Kármán wake is observed. However, the underlying mechanism was found to be different. In their study, the induced LEV on the hind foil, which formed due to the presence of vortex arriving from the fore foil, annihilated later as it reached to the trailing edge at the end of each stroke, unlike what was observed in the current study. On the other hand, in the present study, the lower reduced frequency and higher amplitude, allows the induced LEV to have enough time to reach to the trailing edge before the foil reverses direction. The higher reduced frequency in their study also have caused a narrower jet in the wake of the hind foil, producing higher thrust compared to Ar_1. Despite the differences in kinematics, however, they found a similar ideal phase differences for the spacing of $S = 3c$ ($\phi = 3\pi/2$).

The other extreme configuration of Ar_1, which produced highest drag, appeared at $\phi = 1\pi/4$. Figures 3.8(e) - 3.8(h) illustrate the instantaneous vorticity field. It is shown that at $t/T = 0.50$, TEV-uf arrives at the leading edge of the hind foil when the foil has already started its downstroke. Here, TEV-uf induces an LEV of opposite sign, which subsequently detaches before the foil reaches to the middle point of its downstroke. At $t/T = 0.60$ [Fig. 3.8(f)], continuing the downstroke, it is seen that TEV-uf is overtaking the LEV-uh, while they advect downstream. Later, at $t/T = 0.85$, when the foil is close to the end of downstroke, the detached LEV-uh reaches at the trailing edge. At $t/T = 1.05$, as seen in Fig. 3.8(h), the LEV-uh is broken down in its interaction with the shear layer vortices and the TEV-uf, which has overtaken it. The resulting flow field in Fig. 3.8(h) looks similar to a chaotic drag producing Bénard-Von Kármán vortex street. Fig. 3.7(d) demonstrates the cycle-averaged velocity field of the corresponding configuration.

Model $Ar_{1.5}$: Analyzing the instantaneous flow field of the $Ar_{1.5}$, the reason of its extremely low performance becomes clear. In all configurations of $Ar_{1.5}$, a large vortex shed from the fore foil encounters the tip of the hind foil. As the result of the encounter, the vortex loses its coherence and becomes divided and decomposed into smaller vortices. The difference between the small thrust and high drag producing cases is due to the interactions of the divided vortices with the hind foil, LEV-h and TEV-h. As further analysis of this case

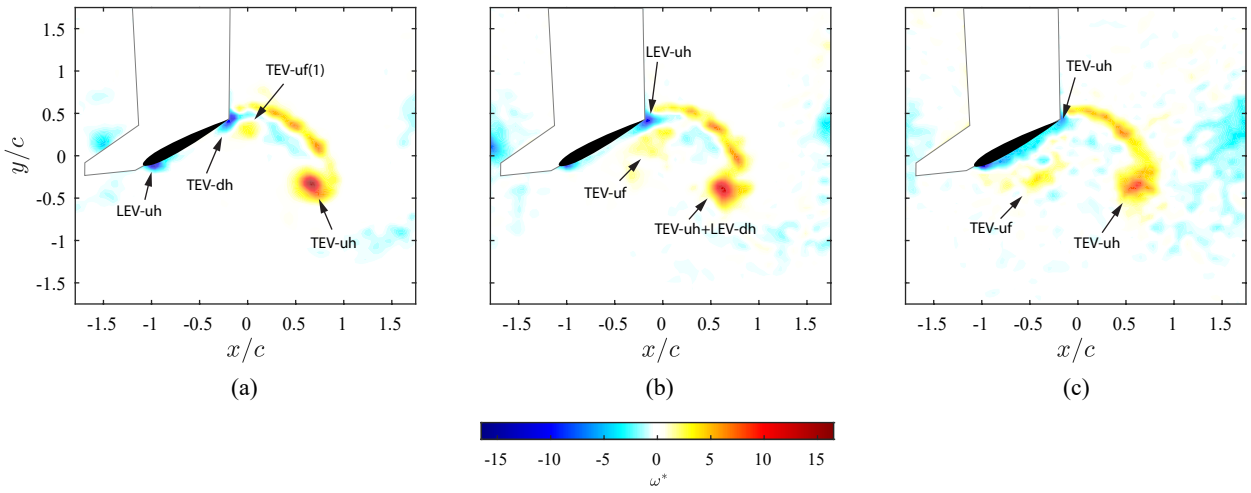

Figure 3.9: Vorticity field of hind foils in highest-performing phase difference of their respective amplitude ratios: (a) $Ar_{0.5}$ at $\phi = 5\pi/4$, (b) Ar_1 at $\phi = 3\pi/2$, and (c) $Ar_{1.5}$ at $\phi = 7\pi/4$. All figures are captured at the beginning of the downstroke.

does little to improve our understanding of the amplitude ratio, plots of the instantaneous flow field of this model over the cycle are not presented. The instantaneous vorticity field of the hind foil at $\phi = 7\pi/4$, which is the highest-thrust producing configuration of the model $Ar_{1.5}$, is shown in the supplementary material, Video 1. The cycle-averaged flow field of high and low performance configurations are presented in Fig. 3.7(e) and 3.7(f).

3.4.5 Comparison of High-Thrust Configurations

To synthesize the observations in previous section, it has been shown that the wake of the fore foil can significantly affect the performance of the hind foil, similar to the observations of previous studies (Boschitsch et al., 2014; Kurt and Moored, 2018; Broering and Lian, 2012; Muscutt et al., 2017a; Xu et al., 2017; Joshi and Mysa, 2021; Kurt et al., 2021). It has been demonstrated that in the high-thrust cases, a vortex pair is formed at the middle of the stroke and is shed at the end of the stroke far from the centerline. This is the underlying mechanism of thrust enhancement for both $Ar_{0.5}$ and Ar_1 configurations. The main effect of this vortex pair in constructive, thrust-enhancing configurations is an increase in TEV strength, and causing alternating TEVs to shed with a greater total wake spacing. Figure 3.9 summarizes the key differences of the underlying mechanisms of thrust augmentation in different amplitude ratio models at their corresponding high-performing cases. In Fig. 3.9

(a) , it is seen that in high-thrust case of $Ar_{0.5}$, the induced *trailing edge vortex* (TEV-dh) contributes to thrust generation. Later this vortex amalgamates with the trailing edge vortex shedding from top surface of the foil forming a stronger trailing edge vortex compared to the one shed from the isolated reference foil. Meanwhile, in the case of Ar_1 it is the induced *leading edge vortex* (LEV-uh) that amalgamates with the trailing edge vortices shed from the top surface, which result in formation of a stronger trailing edge vortex. TEV-uh+LEV-dh in Fig. 3.9(b) denotes this compound vortex shed during the previous stroke (upstroke). As seen in Fig. 3.9 (c), in the model $Ar_{1.5}$, due to the destructive interaction of the high circulation vortex arriving from fore foil (TEV-uf) with the hind foil, the performance of the hind foil is always reduced.

Studying the differences observed in the flow fields of the high-thrust cases of $Ar_{0.5}$ and Ar_1 configurations reveals how $Ar_{0.5}$ produces thrust more effectively than Ar_1. In the high-thrust configuration of Ar_1 ($\phi = 3\pi/2$), the vortex pair that forms on the suction side of the foil is stronger than that forms on $Ar_{0.5}$ at $\phi = 5\pi/4$, which would reduce surface pressure, increasing the total lift on the surface. Although pressure on the foil surface was not determined explicitly, the instantaneous velocity field in Fig. 3.10 reveals a higher velocity in Ar_1, induced due to the presence of stronger vortex pair, which would result in further pressure reduction on the suction side. Given this, as thrust is the component of the instantaneous lift parallel with the free-stream, known as Knoller-Betz effect (Katzmayr, 1922), a higher thrust would be expected for Ar_1 as it generates higher lift. Despite this observation, the higher thrust achieved by $Ar_{0.5}$ at $\phi = 5\pi/4$ can be related to how effectively the wake-foil interaction in this configuration is able to tilt the lift vector in the streamwise direction. Furthermore, the weaker vortex pair on the suction side of the foil in this configuration, would require less power to pitch the foil in comparison to Ar_1 at $\phi = 3\pi/2$, which augments thrust through the foil interaction with a stronger vortex pair.

Analyzing the effect of chord ratio on tandem pitching and heaving foils, Joshi and Mysa (2021) observed reduced performance enhancement of the hind foil by decreasing the reduced frequency (chord size) of the fore foil, due to the reduced energy in the wake of the fore foil. In contrast to their observation, in the present study, higher performance enhancement was achieved by decreasing the Strouhal number of the fore foil (pitch amplitude) and the energy of the flow at the wake of the fore foil. Comparing Fig. 3.6(b), 3.6(d) and 3.6(f), it was observed that the wake of the fore foil in $Ar_{0.5}$ had lower momentum and energy, yet, at

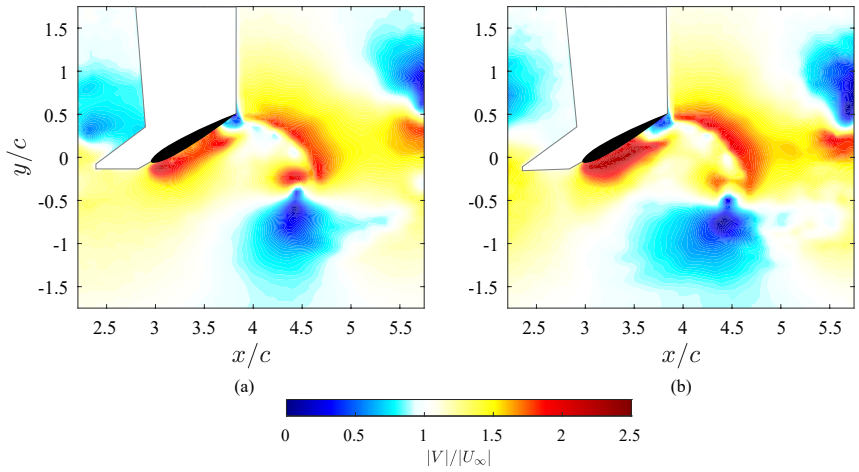

Figure 3.10: Instantaneous velocity magnitude in the flow field of hind foils: (a) $Ar_{0.5}$ at $\phi = 5\pi/4$, and (b) Ar_1 at $\phi = 3\pi/2$. Both figures capture the flow field at $t/T = 0.41$ in the oscillation period of the hind foil.

the optimum phase difference, enhances the performance of the hind more than Ar_1 and $Ar_{1.5}$ at their respective optimum phase differences. Decreasing Strouhal number also causes the wake width of the fore foil to become narrower. As shown in the previous sections, at the optimum phase difference, the hind foil interacts differently with the vortices of the fore foil as the wake width changes. It was observed that as the wake width of the fore foil decreased, thrust augmentation of the hind foil increased at the optimum phase difference. Therefore, the interaction between fore and hind foils cannot be predicted from the time-averaged energy or momentum of the fore-foil wake alone, but their entire time-history of vortex interactions with the hind foil.

3.4.6 Argument on Efficiency

The propulsive efficiency of tandem foils is defined as the ratio of the power gain from the entire system to the total power given to the fluid by the tandem system, known as Froude efficiency,

$$\eta = \frac{\bar{T}}{\bar{P}} = \frac{\bar{C}_{T,M}}{\bar{C}_{P,\mathrm{f}} + \bar{C}_{P,\mathrm{h}}}, \tag{3.2}$$

where η, $\bar{P}$, $\bar{C}_{T,M}$, $\bar{C}_{P,\mathrm{f}}$ and $\bar{C}_{P,\mathrm{h}}$ denote the efficiency, mean power input, mean thrust coefficient of the tandem model, mean power coefficients of fore and hind foils, respectively. In this study, we do not have a direct measurement of the power coefficient, and therefore

cannot give precise values to this efficiency. However, it is possible to cautiously rank the relative efficiency of the high-thrust cases among themselves. It has been shown in the literature that the power coefficient of NACA 0012 airfoil undergoing pure pitching motion excellently scales with St^2k within $500 < Re_c < 32000$ (Senturk and Smits, 2019). Therefore, it is expected that power consumption of the fore foils, which were pitched in isolation, could be ranked based on their Strouhal number according to this scaling. Given the lower Strouhal number of the fore foil in $Ar_{0.5}$ at $\phi = 5\pi/4$, effective thrust production by the hind foil, and the highest thrust achieved among all other configurations, it could be inferred that this configuration likely had higher efficiency than Ar_1 at $\phi = 3\pi/2$. In the same manner, the high-thrust case of Ar_1 ($\phi = 3\pi/2$) likely had higher efficiency than high-thrust configuration of $Ar_{1.5}$ ($\phi = 7\pi/4$) since it produces significantly higher thrust and is expected to consume less energy in comparison. However, to confirm these speculations, explicit studies regarding the effect of amplitude ratio on efficiency are required.

In addition to the reasoning discussed above, the same observation can be inferred from the results of other studies. In the literature, it has been shown that the high thrust and high efficiency are achieved approximately concurrently in tandem in-line propulsors regardless of their motion type (pure pitching (Boschitsch et al., 2014) or pitching and heaving (Muscutt et al., 2017a,b)). In fact, this has been shown as one of the advantages of the tandem propulsors over isolated ones where high values of thrust are obtained at the price of lower efficiency. Joshi and Mysa (2021) showed that for higher thrust producing configuration, higher efficiency has been achieved at all chord ratios of tandem foils despite an energy reduction in the wake of fore foil at smaller chord ratios. Therefore, there is a very high probability that highest thrust producing configuration of this study is nearly in phase with high efficiency. Conservatively, it can be suggested that a rear-biased locomotion could be more beneficial for a natural or a man-made vehicle employing tandem propulsion system. A future, targeted study on efficiency may confirm this suggestion.

In the paleontological context, our results indicate that plesiosaurs could likely achieve higher performance and efficiency if they had moved their hind flippers at larger amplitudes than fore flippers in cruising conditions. This suggestion is consistent with the fossil records of pliosaurs which had more developed pelvic girdles (O'Keefe, 2002; O'Keefe and Carrano, 2005) and are thought to be pursuit predators (Taylor, 1981; Massare, 1988). However, our findings are not consistent with the fossil records of long-necked, small-headed plesiosaurs,

which show higher angular amplitude range for the fore flipper (Liu et al., 2015; Carpenter et al., 2010), and a more massive development of the pectoral (shoulder) girdle when compared to hind foil (O'Keefe, 2002; O'Keefe and Carrano, 2005). We anticipate that although the propulsive performance was important for plesiosaurs, there were other selective pressures than efficiency for exhibiting almost identical flippers with different morphologies. However, this cannot be generalized to all plesiosaur specimens as they were diverse group of animals within their clades. Any further claims based on the results of the present study likely require a species-specific analysis, considering paleontological and biological aspects of plesiosaurs. However, the findings of this study might inform such future studies on plesiosaur locomotion.

3.5 Summary and Conclusions

Inspired by the kinematics of plesiosaur flippers, PIV experiments have been conducted on two tandem pitching hydrofoils undergoing sinusoidal oscillations at high amplitudes to study the effect of amplitude ratio on the propulsive performance. Three models of $Ar_{0.5}$, Ar_1 and $Ar_{1.5}$ studied on a range of $0 < \phi < 2\pi$ for a fixed spacing of $S = 3c$. For the first time, it has been shown that the effect of amplitude ratio on the thrust generation of hind foil is significant for spacing of $S > 1c$. Control volume analysis revealed that when the amplitude ratio was set to 0.5, highest thrust among all configurations was achieved at $\phi = 5\pi/4$, confirming our hypothesis. For this configuration, the total thrust coefficient reaches as high as 2.3 times those of an isolated foil pitching with the kinematics of the hind foil. The total thrust achieved by $Ar_{0.5}$ at $\phi = 5\pi/4$ was also 10% higher than the highest thrust producing case of amplitude ratio of Ar_1 at ($\phi = 3\pi/2$). The superiority of the total tandem system performance of $Ar_{0.5}$ configurations was evident over the entire phase difference domain. Increasing amplitude ratio to 1.5 was found to have detrimental effects on the performance of the hind foil producing negligible thrust at $\phi = 7\pi/4$ and high drag in all other configurations. It was observed that for a fixed spacing between the foils, by changing the amplitude ratio the optimum phase difference shifts.

Instantaneous vorticity field analysis showed that the highest-thrust configurations of $Ar_{0.5}$ and Ar_1 exhibit almost similar wakes where the vortices are stronger and positioned at a higher lateral distance from the centerline compared to the reference foil's wake. The time

averaged of this reverse Bénard-Von Kármán vortex street illustrates a high momentum jet in the wake of the hind foil. The underlying mechanism of such wake was found to be the formation of a vortex pair at the middle and its shedding at the end of each stroke. This vortex pair consisted of TEV arriving from the fore foil and TEV (in case of $Ar_{0.5}$) or LEV (in case of Ar_1) induced on the suction side of the hind foil. It is observed as the wake width of the fore foil decreased with amplitude ratio, the hind foil experienced different types of wake-foil interactions to enhance thrust at the corresponding optimum phase difference. Further comparative analysis on the wake showed that the hind foil in high-thrust configuration of $Ar_{0.5}$ produces thrust more effectively than the one in Ar_1. Significantly low performance of all configurations of $Ar_{1.5}$ model was identified to be associated with destructive encounter of hind foil with a large vortex shed from the fore foil for all phase differences studied in this model.

The results of this study suggest that hind foil in a rear-biased propulsion system benefits from enhanced performance. Although the power input to the foils was not measured explicitly in this study, using the scaling suggested by Senturk and Smits (2019) for pitching NACA 0012 foils, a relative efficiency ranking between the highest-thrust configurations of the tandem models was made possible. Based on the hypothetical ranking, it was argued that $Ar_{0.5}$ at $\phi = 5\pi/4$ was more efficient than the other high-thrust configurations, therefore suggesting that a rear-biased propulsion system was more efficient. Direct measurement of power is required to confirm this suggestion. The findings of this study may inform future studies on plesiosaur swimming and efficient marine/aerial vehicle design. The present work may be extended to include effect of heave amplitude ratio, frequency ratio, cross-stream spacing between the foils and three dimensionality on the performance of the tandem propulsors to model more realistic biological locomotion.

Chapter 4

Summary and Conclusion

The locomotion strategies of plesiosaurs has been an open question since they were discovered. Understanding their locomotion would provide useful insights on the behavior of these enigmatic, giant animals, which have no living analogue today. Nature has always been a great source of inspiration for innovation in engineering, as it provides endless interesting solutions for complex problems. Understanding the biological locomotion of animals, extinct or otherwise, is not an exception, and it can help engineers to design and develop more efficient marine and aerial vehicles. In our case, the unique case of nearly-identical wing-like fore and hind flippers of plesiosaurs, which remained consistent throughout their evolution and diversification within the clade, may imply an effectiveness and efficiency of such propulsors. Motivated by this mystery, in this thesis we attempted to predict the maneuverability of plesiosaurs in Chapter 2, while in Chapter 3 we experimentally investigated the role of hind flippers. A new optimizing factor for efficient cruising in a tandem propulsion system, the amplitude ratio, was identified in Chapter 3. In this chapter, the findings of preceding chapters are summarized, and a collective insight obtained by considering their findings together is presented, which will further enhance our understanding of plesiosaur behavior and locomotion. Finally, the potential avenues for future investigations are identified from the limitations of the current work.

4.1 Plesiosaur Behavior

In Chapter 2, the behavior of plesiosaurs was predicted using universal scaling rules for fluid mechanics. Reduced frequency was considered as a metric for agility in flapping species. The equation for reduced frequency was modified such that it can be calculated as function

of the Strouhal number and from the purely geometric data which can be measured from plesiosaur fossils:

$$k = St\frac{\pi c}{\theta_0 b}. \tag{4.1}$$

This modified relation was validated for flapping species from a range of environments, ranging from insects to marine mammals. This showed that the above relation for reduced frequency is robust given a known flapping angle. In order to determine how well a flapping angle from fossil data could be predicted, it was applied to a sea turtle. In that example, the reduced frequency of a sea turtle utilizing direct measurements of the skeleton from computed tomography x-ray data was predicted within a 4% difference from that observed in nature.

Following the validation of this methodology, the reduced frequency of low, moderate, and high aspect ratio plesiosaurs was calculated. It was revealed that plesiosaurs with high aspect ratios (plesiosauroids), similar to sea turtles and albatrosses, had lower agility and a limited level of maneuverability compared to plesiosaurs with lower aspect ratios (pliosauroids), which had reduced frequencies similar to that of penguins and hummingbirds, which are capable of rapid manoeuvres. This finding was found to be consistent with previous literature categorizing plesiosaur's maneuverability and hunting style based on the neck length as a limiting factor.

4.2 Optimum Swimming Strategies

In the literature, as presented in Chapter 1, it has been argued that plesiosaurs would have performed underwater flight (lift based propulsion as opposed to drag based propulsion) for swimming due to the resemblance of plesiosaur flippers to hydrodynamic planforms and the possible flipper motions determined from physical measurements on fossils. This type of propulsion can be abstracted using pitching foils. To further understand the plesiosaur locomotion, PIV experiments were conducted on tandem pitching NACA 0012 airfoils. Inspired by the difference in morphologies of fore and hind flippers in plesiosaurs, the effect of amplitude ratio on propulsive performance was investigated for tandem pitching foils.

It has been demonstrated that amplitude ratio can significantly affect the performance of the hind flipper in an in-line tandem pitching configuration, introducing a new optimizing

factor for tandem propulsion systems. It has been revealed that rear-biased locomotion likely would have been more beneficial for plesiosaurs as the hind foil produced higher thrust and the tandem system reached relatively higher efficiency at the optimum phase angle. Such a model is consistent with flipper morphologies of short-necked plesiosaurs (pliosauroids), which exhibit more developed pelvic girdles, larger femurs, and even slightly larger hind flippers in some specimens. However, it was not consistent with the fossil records observed in long-necked plesiosaurs (plesiosauroids), which had more developed pectoral girdles and larger humeri. Furthermore, a forward-biased configuration inspired by such morphologies, was observed to have detrimental effect on the performance of the hind flipper for all phase differences. Although, the equal-amplitude propulsion could be an efficient choice of locomotion for plesiosaurs with long necks (plesiosauroids), it does not account for the massive development of the shoulder girdles and the evidence for large muscles origination on the chest and inserting on the humeri.

In Chapter 3, the instantaneous velocity and vorticity fields revealed that the hind flippers produced thrust more effectively when they were pitched at twice amplitude of the fore foils compared to the ones in equal-amplitude configurations. It was argued that the amplitude ratio changes the wake spacing seen by the hind foil, which alters the wake-foil interactions. In the optimum phase difference of rear-biased and equal amplitude models, following the wake-foil interactions, stronger trailing edge vortices were shed with greater cross-stream spacing in the wake of the hind foils. These findings can provide a base-line for future studies aiming to design and develop more efficient tandem foil systems.

4.3 So, How Did Plesiosaurs Swim?

In the absence of a living analogue, the answer to this question might remain elusive. However, in continuation of the attempts of previous literature to shed light on biological locomotion, particularly plesiosaur locomotion, this thesis provides new insights. The findings in Chapter 3 indicate that likely both fore and hind sets of flippers should have been involved in locomotion to ensure an efficient propulsion, rather than a single set, supporting the findings of Muscutt et al. For short-necked, large-headed plesiosaurs (pliosauroids), exhibiting more developed pelvic girdles and femurs, the high agility level suggested in Chapter 2 was confirmed by the findings in Chapter 3, which illustrated that a rear-biased locomotion

could have resulted in higher thrust production, which is critical to both powerful initial acceleration and rapid turning. These properties are what a pursuit predator with high maneuverability would require, which are attributed to pliosauroids based on the ecological niche implied by fossil records. In the case of long-necked, small-headed plesiosaurs (plesiosauroids), although they could possibly have used this strategy for high thrust generation, such as during escape, the fossil data provides no evidence for chosing a rear-biased propulsion system over other strategies. As forward-biased propulsion did not exceedsingle-foil performance, it is possible that they simply did not use their hind flippers. It is speculated that despite the importance of efficiency for these types of plesiosaurs, other selective pressures might have played a role resulting in development of identical flippers with different morphologies. For example, they might have needed it for limited propuslive use, such as occasional escape maneovures. Furthermore, this supports the findings in Chapter 2 that agreed with the catagorization of plesiosauroids as ambush predators, due to their likely limited level of agility.

As highlighted in Chapter 3, the results and findings of this thesis are general statements of airfoil flows, and cannot be applied to all specimens of plesiosaurs equally, as they were highly diverse animals within their clade. Any specific conclusions on their locomotion based on the observations presented here would likely require a species-specific analysis.

4.4 Future Work

Following the findings of this thesis, many new questions arise, which could enhance our understanding of biological locomotion. Previously it was thought the most important parameter determining the performance of tandem flippers was the phase difference and spacing between the foils. As shown in this study, amplitude ratio has no less an effect than the prementioned parameters. Therefore, investigating the effect of amplitude ratio and frequency ratio on propulsive performance of tandem oscillating (pitching, heaving, or combination of both) foils over a larger parameter space would result in identification of a new optimum configuration. Furthermore, the results of such an investigation may be helpful in identification of a relation between the cross-stream wake spacing seen by the hind foil and its propulsive performance. This can potentially help the development of more efficient aerial and marine vehicles.

Performing experiments or numerical simulations with realistic flippers undergoing realistic flipper motion, as measured from plesiosaur fossils, may further improve our knowledge of plesiosaur locomotion. Considering the effect of aspect ratio (and therefore other three-dimensional effects) can provide further support for the findings of Chapter 2. Particularly for plesiosauroids, considering the asymmetric flapping motion would probably help reveal the reason behind the massive development of shoulder girdles. Although it is thought that spanwise and chordwise flexibility might have secondary effects in swimming in cruising conditions, introducing their effect in the investigation may provide insights about plesiosaurs' maneuverability .

4.5 Closing Remarks

Swimming behavior of plesiosaurs has been questioned for more than three centuries. This thesis investigated their behavior from hydrodynamics perspective. Although the findings of this study provide new insights to this subject, we are far from the point to fully comprehend the locomotion of these enigmatic giants. However, it is hoped through the small increments such as presented here, the mystery of their locomotion become revealed.

Bibliography

I. Akhtar, R. Mittal, G. V. Lauder, and E. Drucker. Hydrodynamics of a biologically inspired tandem flapping foil configuration. *Theoretical and Computational Fluid Dynamics*, 21(3): 155–170, 2007.

R. Allemand, N. Bardet, A. Houssaye, and P. Vincent. New plesiosaurian specimens (reptilia, plesiosauria) from the upper cretaceous (turonian) of goulmima (southern morocco). *Cretaceous Research*, 82:83–98, 2018.

J. M. Anderson, K. Streitlien, D. Barrett, and M. S. Triantafyllou. Oscillating foils of high propulsive efficiency. *Journal of Fluid mechanics*, 360:41–72, 1998.

C. W. Andrews. *A Descriptive Catalogue of the Marine Reptiles of the Oxford Clay: Based on the Leeds Collection in the British Museum (Natural History) Library, London*, volume 2. order of the Trustees of the British Museum, 1913.

H. Aono, W. Shyy, and H. Liu. Near wake vortex dynamics of a hovering hawkmoth. *Acta Mechanica Sinica*, 25(1):23–36, 2009.

R. Araújo and F. Correia. Soft-tissue anatomy of the plesiosaur pectoral girdle inferred from basal eosauropterygia taxa and the extant phylogenetic bracket. *Palaeontologia Electronica*, 18(1):1–32, 2015.

R. Araújo, M. J. Polcyn, A. Schulp, O. Mateus, L. Jacobs, A. O. Gonçalves, and M.-L. Morais. A new elasmosaurid from the early maastrichtian of angola and the implications of girdle morphology on swimming style in plesiosaurs. *Netherlands Journal of Geosciences*, 94(1):109–120, 2015.

Y. S. Baik, L. P. Bernal, K. Granlund, and M. V. Ol. Unsteady force generation and vortex dynamics of pitching and plunging aerofoils. *Journal of Fluid Mechanics*, 709:37–68, 2012.

R. B. Benson, M. Evans, and P. S. Druckenmiller. High diversity, low disparity and small body size in plesiosaurs (reptilia, sauropterygia) from the triassic–jurassic boundary. *PLoS One*, 7(3):e31838, 2012.

R. B. Benson, H. F. Ketchum, D. Naish, and L. E. Turner. A new leptocleidid (sauropterygia, plesiosauria) from the vectis formation (early barremian–early aptian; early cretaceous) of the isle of wight and the evolution of leptocleididae, a controversial clade. *Journal of Systematic Palaeontology*, 11(2):233–250, 2013.

C. Betts and R. Wootton. Wing shape and flight behaviour in butterflies (lepidoptera: Papilionoidea and hesperioidea): a preliminary analysis. *Journal of experimental biology*, 138(1):271–288, 1988.

A. Betz. Ein beitrag zur erklaerung segelfluges. *Z Flugtech Motorluftschiffahrt*, 3:269–272, 1912.

W. Birnbaum. Das ebene problem des schlagenden flügels. *ZAMM-Journal of Applied Mathematics and Mechanics/Zeitschrift für Angewandte Mathematik und Mechanik*, 4(4): 277–292, 1924.

D. G. Bohl and M. M. Koochesfahani. Mtv measurements of the vortical field in the wake of an airfoil oscillating at high reduced frequency. *Journal of Fluid Mechanics*, 620:63–88, 2009.

B. M. Boschitsch, P. A. Dewey, and A. J. Smits. Propulsive performance of unsteady tandem hydrofoils in an in-line configuration. *Physics of Fluids*, 26(5):051901, 2014.

T. M. Broering and Y.-S. Lian. The effect of phase angle and wing spacing on tandem flapping wings. *Acta Mechanica Sinica*, 28(6):1557–1571, 2012.

T. M. Broering, Y. Lian, and W. Henshaw. Numerical investigation of energy extraction in a tandem flapping wing configuration. *AIAA journal*, 50(11):2295–2307, 2012.

R. Bullen and N. McKenzie. Scaling bat wingbeat frequency and amplitude. *Journal of experimental biology*, 205(17):2615–2626, 2002.

K. Carpenter, F. Sanders, B. Reed, J. Reed, and P. Larson. Plesiosaur swimming as interpreted from skeletal analysis and experimental results. *Transactions of the Kansas Academy of Science*, 113(1/2):1–34, 2010.

T. Cebeci, M. Platzer, H. Chen, K.-C. Chang, and J. P. Shao. *Analysis of low-speed unsteady airfoil flows*. Springer, 2005.

H. W. Coleman and W. G. Steele. *Experimentation, validation, and uncertainty analysis for engineers*. John Wiley & Sons, 2018.

S. Combes and T. Daniel. Shape, flapping and flexion: wing and fin design for forward flight. *Journal of experimental biology*, 204(12):2073–2085, 2001.

L. Cong, B. Teng, and L. Cheng. Hydrodynamic behavior of two-dimensional tandem-arranged flapping flexible foils in uniform flow. *Physics of Fluids*, 32(2):021903, 2020.

L. N. Cooper, A. Berta, S. D. Dawson, and J. S. Reidenberg. Evolution of hyperphalangy and digit reduction in the cetacean manus. *The Anatomical Record: Advances in Integrative Anatomy and Evolutionary Biology: Advances in Integrative Anatomy and Evolutionary Biology*, 290(6):654–672, 2007.

J. O. Dabiri. Optimal vortex formation as a unifying principle in biological propulsion. *Annual review of fluid mechanics*, 41:17–33, 2009.

J. Davenport, S. A. Munks, and P. Oxford. A comparison of the swimming of marine and freshwater turtles. *Proceedings of the Royal society of London. Series B. Biological sciences*, 220(1221):447–475, 1984.

E. G. Drucker and G. V. Lauder. Locomotor function of the dorsal fin in teleost fishes: experimental analysis of wake forces in sunfish. *Journal of Experimental Biology*, 204(17): 2943–2958, 2001.

R. Dudley. Biomechanics of flight in neotropical butterflies: morphometrics and kinematics. *Journal of Experimental Biology*, 150(1):37–53, 1990.

A. R. Ennos. The kinematics and aerodynamics of the free flight of some diptera. *Journal of Experimental Biology*, 142(1):49–85, 1989.

V. Fischer, R. B. Benson, P. S. Druckenmiller, H. Ketchum, and N. Bardet. The evolutionary history of polycotylid plesiosaurians. *Royal Society open science*, 5(3):172177, 2018.

F. E. Fish. Comparative kinematics and hydrodynamics of odontocete cetaceans: morphological and ecological correlates with swimming performance. *The Journal of Experimental Biology*, 201(20):2867–2877, 1998.

F. E. Fish, S. Innes, and K. Ronald. Kinematics and estimated thrust production of swimming harp and ringed seals. *Journal of Experimental Biology*, 137(1):157–173, 1988.

D. Floryan, T. Van Buren, and A. J. Smits. Efficient cruising for swimming and flying animals is dictated by fluid drag. *Proceedings of the National Academy of Sciences*, 115 (32):8116–8118, 2018.

E. Frey and J. Riess. Considerations concerning plesiosaur locomotion. *Neues Jahrbuch für Geologie und Paläontologie-Abhandlungen*, pages 193–194, 1982.

M. Gharib, E. Rambod, and K. Shariff. A universal time scale for vortex ring formation. *Journal of Fluid Mechanics*, 360:121–140, 1998.

S. J. Godfrey. Plesiosaur subaqueous locomotion-a reappraisal. *Neues Jahrbuch für Geologie und Paläontologie-Monatshefte*, pages 661–672, 1984.

R. Godoy-Diana, J.-L. Aider, and J. E. Wesfreid. Transitions in the wake of a flapping foil. *Physical Review E*, 77(1):016308, 2008.

A. Gungor, M. S. U. Khalid, and A. Hemmati. How does switching synchronization of pitching parallel foils from out-of-phase to in-phase change their wake dynamics? *Physics of Fluids*, 33(8):081901, 2021.

L. Halstead. Plesiosaur locomotion. *Journal of the Geological Society*, 146(1):37–40, 1989.

C. Hartloper, M. Kinzel, and D. E. Rival. On the competition between leading-edge and tip-vortex growth for a pitching plate. *Experiments in fluids*, 54(1):1–11, 2013.

S. Heathcote and I. Gursul. Flexible flapping airfoil propulsion at low reynolds numbers. *AIAA journal*, 45(5):1066–1079, 2007.

D. M. Henderson. The eyes have it: the sizes, shapes, and orientations of theropod orbits as indicators of skull strength and bite force. *Journal of Vertebrate Paleontology*, 22(4): 766–778, 2003.

D. M. Henderson. Floating point: a computational study of buoyancy, equilibrium, and gastroliths in plesiosaurs. *Lethaia*, 39(3):227–244, 2006.

P. Henningsson, G. Spedding, and A. Hedenstrom. Vortex wake and flight kinematics of a swift in cruising flight in a wind tunnel. *Journal of Experimental Biology*, 211(5):717–730, 2008.

T. L. Hilderman. *Measurement, modelling, and stochastic simulation of concentration fluctuations in a shear flow*. Ph.D. thesis, University of Alberta, Department of Mechanical Engineering, 2004.

D. Hummel. Aerodynamic aspects of formation flight in birds. *Journal of theoretical biology*, 104(3):321–347, 1983.

K. Jones, C. Dohring, and M. Platzer. Experimental and computational investigation of the knoller-betz effect. *AIAA journal*, 36(7):1240–1246, 1998.

V. Joshi and R. C. Mysa. Mechanism of wake-induced flow dynamics in tandem flapping foils: Effect of the chord and gap ratios on propulsion. *Physics of Fluids*, 33(8):087104, 2021.

R. Katzmayr. Effect of periodic changes of angle of attack on behavior of airfoils. Technical report, 1922.

R. Knoller and O. Verein. Die gesetze des luftwiderstandes. verlag des osterreichischer flugtechnischen vereines, 1909.

M. M. Koochesfahani. Vortical patterns in the wake of an oscillating airfoil. *AIAA journal*, 27(9):1200–1205, 1989.

A. Krahl. The locomotory apparatus and paraxial swimming in fossil and living marine reptiles: comparing nothosauroidea, plesiosauria, and chelonioidea. *PalZ*, 95(3):483–501, 2021.

A. Krahl and U. Witzel. Foreflipper and hindflipper muscle reconstructions of cryptoclidus eurymerus in comparison to functional analogues: introduction of a myological mechanism for flipper twisting. *PeerJ*, 9:e12537, 2021.

T. Kubo, M. T. Mitchell, and D. M. Henderson. Albertonectes vanderveldei, a new elasmosaur (reptilia, sauropterygia) from the upper cretaceous of alberta. *Journal of Vertebrate Paleontology*, 32(3):557–572, 2012.

M. Kurt and K. W. Moored. Flow interactions of two-and three-dimensional networked bio-inspired control elements in an in-line arrangement. *Bioinspiration & biomimetics*, 13(4): 045002, 2018.

M. Kurt, A. Mivehchi, and K. Moored. High-efficiency can be achieved for non-uniformly flexible pitching hydrofoils via tailored collective interactions. *Fluids*, 6(7):233, 2021.

C. LeBuff. The loggerhead turtle in the eastern gulf of mexico, caretta. *Research Inc., Sanibel, Florida*, 216, 1990.

Z.-Y. Li, L.-H. Feng, J. Kissing, C. Tropea, and J.-J. Wang. Experimental investigation on the leading-edge vortex formation and detachment mechanism of a pitching and plunging plate. *Journal of Fluid Mechanics*, 901, 2020.

T. Lingham-Soliar. Plesiosaur locomotion: is the four-wing problem real or merely an atheoretical exercise? *Neues Jahrbuch für Geologie und Paläontologie-Abhandlungen*, pages 45–87, 2000.

P. B. Lissaman and C. A. Shollenberger. Formation flight of birds. *Science*, 168(3934): 1003–1005, 1970.

G. Liu, Y. Ren, H. Dong, O. Akanyeti, J. C. Liao, and G. V. Lauder. Computational analysis of vortex dynamics and performance enhancement due to body–fin and fin–fin interactions in fish-like locomotion. *Journal of fluid mechanics*, 829:65–88, 2017.

S. Liu, A. S. Smith, Y. Gu, J. Tan, C. K. Liu, and G. Turk. Computer simulations imply forelimb-dominated underwater flight in plesiosaurs. *PLoS Computational Biology*, 11(12): e1004605, 2015.

K. N. Lucas, G. V. Lauder, and E. D. Tytell. Airfoil-like mechanics generate thrust on the anterior body of swimming fishes. *Proceedings of the National Academy of Sciences*, 117 (19):10585–10592, 2020.

J. A. Massare. Swimming capabilities of mesozoic marine reptiles: implications for method of predation. *Paleobiology*, 14(2):187–205, 1988.

L. Muscutt. *The Hydrodynamics of Plesiosaurs*. Ph.D. thesis, University of Southampton, 2017.

L. Muscutt, G. Weymouth, and B. Ganapathisubramani. Performance augmentation mechanism of in-line tandem flapping foils. *Journal of Fluid Mechanics*, 827:484–505, 2017a.

L. E. Muscutt, G. Dyke, G. D. Weymouth, D. Naish, C. Palmer, and B. Ganapathisubramani. The four-flipper swimming method of plesiosaurs enabled efficient and effective locomotion. *Proceedings of the Royal Society B: Biological Sciences*, 284(1861):20170951, 2017b.

B. Newman and L. Tarlo. A giant marine reptile from bedfordshire. *Animals*, 10(2):61–63, 1967.

F. R. O'Keefe. The evolution of plesiosaur and pliosaur morphotypes in the plesiosauria (reptilia: Sauropterygia). *Paleobiology*, 28(1):101–112, 2002.

F. R. O'Keefe and M. T. Carrano. Correlated trends in the evolution of the plesiosaur locomotor system. *Paleobiology*, 31(4):656–675, 2005.

C. Pennycuick. Wingbeat frequency of birds in steady cruising flight: new data and improved predictions. *The Journal of experimental biology*, 199(7):1613–1618, 1996.

M. Raffel, C. E. Willert, and J. Kompenhans. *Particle image velocimetry: a practical guide*. Springer International Publishing AG, Cham, Switzerland, 3rd edition, 2018.

D. A. Read, F. Hover, and M. Triantafyllou. Forces on oscillating foils for propulsion and maneuvering. *Journal of Fluids and Structures*, 17(1):163–183, 2003.

D. Rival, G. Hass, and C. Tropea. Recovery of energy from leading-and trailing-edge vortices in tandem-airfoil configurations. *Journal of Aircraft*, 48(1):203–211, 2011.

J. A. Robinson. The locomotion of plesiosaurs. *Neues Jahrbuch fur Mineralogie Geologie und Palaontologie, Abhandlungen*, 149:286–332, 1975.

J. A. Robinson. Intracorporal force transmission in plesiosaurs. *Neues Jahrbuch fur Mineralogie Geologie und Palaontologie, Abhandlungen*, 153:86–128, 1977.

M. Rosén, G. Spedding, and A. Hedenstrom. The relationship between wingbeat kinematics and vortex wake of a thrush nightingale. *Journal of Experimental Biology*, 207(24):4255–4268, 2004.

G. Rüppell. Kinematic analysis of symmetrical flight manoeuvres of odonata. *Journal of experimental Biology*, 144(1):13–42, 1989.

E. Salami, T. A. Ward, E. Montazer, and N. N. N. Ghazali. A review of aerodynamic studies on dragonfly flight. *Proceedings of the Institution of Mechanical Engineers, Part C: Journal of Mechanical Engineering Science*, 233(18):6519–6537, 2019.

K. Sato, K. Shiomi, Y. Watanabe, Y. Watanuki, A. Takahashi, and P. J. Ponganis. Scaling of swim speed and stroke frequency in geometrically similar penguins: they swim optimally to minimize cost of transport. *Proceedings of the Royal Society B: Biological Sciences*, 277 (1682):707–714, 2010.

U. Senturk and A. J. Smits. Reynolds number scaling of the propulsive performance of a pitching airfoil. *Aiaa Journal*, 57(7):2663–2669, 2019.

G. Spedding. The wake of a kestrel (falco tinnunculus) in flapping flight. *Journal of experimental biology*, 127(1):59–78, 1987.

O. Stalnov, H. Ben-Gida, A. J. Kirchhefer, C. G. Guglielmo, G. A. Kopp, A. Liberzon, and R. Gurka. On the estimation of time dependent lift of a european starling (sturnus vulgaris) during flapping flight. *PLoS One*, 10(9):e0134582, 2015.

G. W. Storrs. Function and phylogeny in sauropterygian (diapsida) evolution. *American Journal of Science*, 293(A):63, 1993.

W. Stukeley. Iii. an account of the impression of the almost entire sceleton of a large animal in a very hard stone, lately presented the royal society, from nottinghamshire. *Philosophical Transactions of the Royal Society of London*, 30(360):963–968, 1719.

S. Tarsitano and J. Riess. Plesiosaur locomotion-underwater flight versus rowing. *Neues Jahrbuch für Geologie und Paläontologie-Abhandlungen*, pages 188–192, 1982.

G. K. Taylor, R. L. Nudds, and A. L. Thomas. Flying and swimming animals cruise at a strouhal number tuned for high power efficiency. *Nature*, 425(6959):707–711, 2003.

M. A. Taylor. Plesiosaurs-rigging and ballasting. *Nature*, 290(5808):628–629, 1981.

B. W. Tobalske, D. R. Warrick, C. J. Clark, D. R. Powers, T. L. Hedrick, G. A. Hyder, and A. A. Biewener. Three-dimensional kinematics of hummingbird flight. *Journal of Experimental Biology*, 210(13):2368–2382, 2007.

M. Triantafyllou, G. Triantafyllou, and R. Gopalkrishnan. Wake mechanics for thrust generation in oscillating foils. *Physics of Fluids A: Fluid Dynamics*, 3(12):2835–2837, 1991.

P. V. Troelsen, D. M. Wilkinson, M. Seddighi, D. R. Allanson, and P. L. Falkingham. Functional morphology and hydrodynamics of plesiosaur necks: does size matter? *Journal of Vertebrate Paleontology*, 39(2):e1594850, 2019.

J. Videler and P. Kamermans. Differences between upstroke and downstroke in swimming dolphins. *Journal of Experimental Biology*, 119(1):265–274, 1985.

T. Von Karman and J. Burgers. General aerodynamic theory-perfect fluids," division e, vol. ii, aerodynamic theory, ed. *Durand, WF*, 308, 1943.

J. A. Walker and M. W. Westneat. Mechanical performance of aquatic rowing and flying. *Proceedings of the Royal Society of London. Series B: Biological Sciences*, 267(1455):1875–1881, 2000.

D. Watson. The elasmosaurid shoulder-girdle and fore-limb. In *Proceedings of the Zoological Society of London*, volume 94, pages 885–917. Wiley Online Library, 1924.

D. Weihs. Hydromechanics of fish schooling. *Nature*, 241(5387):290–291, 1973.

D. Weihs and W. TYT. Swimming and flying in nature, 1975.

R. Wilson and N. Liebsch. Up-beat motion in swinging limbs: new insights into assessing movement in free-living aquatic vertebrates. *Marine Biology*, 142(3):537–547, 2003.

T. Wintrich, S. Hayashi, A. Houssaye, Y. Nakajima, and P. M. Sander. A triassic plesiosaurian skeleton and bone histology inform on evolution of a unique body plan. *Science Advances*, 3(12):e1701144, 2017.

T. Wintrich, R. Jonas, H.-J. Wilke, L. Schmitz, and P. M. Sander. Neck mobility in the jurassic plesiosaur cryptoclidus eurymerus: finite element analysis as a new approach to understanding the cervical skeleton in fossil vertebrates. *PeerJ*, 7:e7658, 2019.

M. Wolfgang, J. Anderson, M. Grosenbaugh, D. Yue, and M. Triantafyllou. Near-body flow dynamics in swimming fish. *Journal of Experimental Biology*, 202(17):2303–2327, 1999.

J. G. Wong and D. E. Rival. Determining the relative stability of leading-edge vortices on nominally two-dimensional flapping profiles. *Journal of Fluid Mechanics*, 766:611–625, 2015.

J. G. Wong, A. Mohebbian, J. Kriegseis, and D. E. Rival. Rapid flow separation for transient inflow conditions versus accelerating bodies: An investigation into their equivalency. *Journal of Fluids and Structures*, 40:257–268, 2013.

X. Wu, X. Zhang, X. Tian, X. Li, and W. Lu. A review on fluid dynamics of flapping foils. *Ocean Engineering*, 195:106712, 2020.

G. Xu, W. Duan, and W. Xu. The propulsion of two flapping foils with tandem configuration and vortex interactions. *Physics of Fluids*, 29(9):097102, 2017.

H. Yu, X.-Y. Lu, and H. Huang. Collective locomotion of two uncoordinated undulatory self-propelled foils. *Physics of Fluids*, 33(1):011904, 2021.

Appendix A

A.1 Supplementary Data

In this section, supplementary data supporting the findings in Chapter 2 are presented.

Table A.1: Flapping angle and frequency of sea turtles swimming in cruising conditions measured from online videos.

Speciemen	Flapping Angle (deg)	Frequency (Hz)
Caretta Caretta	120	0.47
Chelonia Mydas	124.63	0.36
Unkown	120.78	0.31
Unknown	127.92	
Unknown	113.45	0.24
Caretta Caretta	126.01	0.3
Average	122.13	0.33

Table A.2: Flapping angle and aspect ratio of sea turtles measured from 3D reconstructed skeleton from CT scans.

Specimen	Flapping angle (deg)	Aspect ratio
Caretta Caretta	133.67	3.76
Caretta Caretta	133.99	
Chelonia Mydas	138.87	
Eretmochelys Imbricata	140.18	
Average flapping angle	136.67	

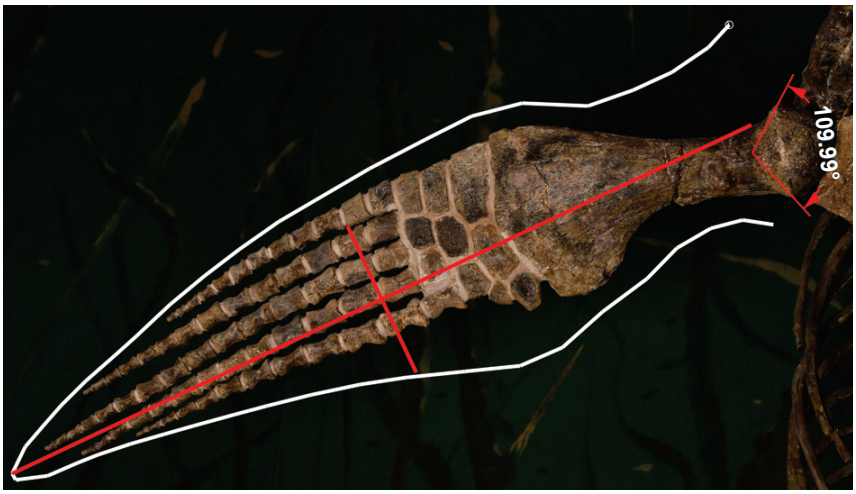

Figure A.1: Fore flipper of *Trinacomerum osbornii*. Outlining and measuring flipper area and span and measuring the flapping angle from the angular extent of proximal end of humerus from scapulohumeral joint.

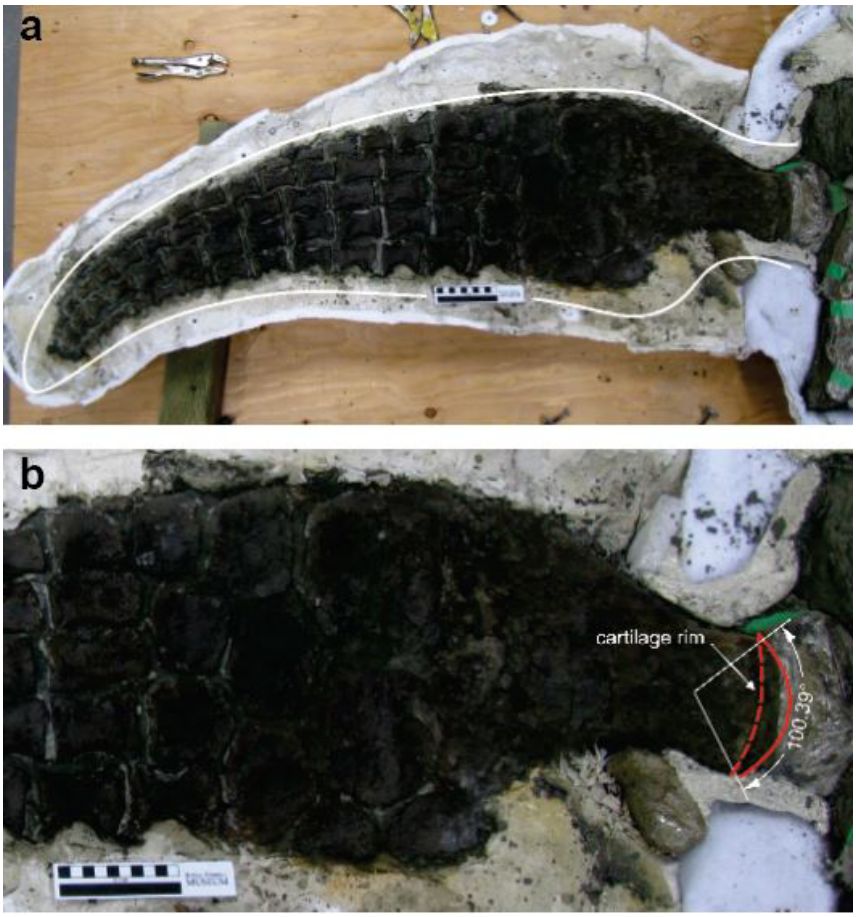

Figure A.2: Fore flipper of Parson's Creek. (a) Outlining and measuring flipper area and span. (b) Measuring the flapping angle from the angular extent of proximal end of humerus from scapulohumeral joint.

Table A.3: Skeletal measurements of plesiosaurs.

Specimen	Notes	Wing span	Wing area	Flapping angle (deg)	AR	Chord
Albertonectes vanderveldei	forelimb	2.13 m	0.71 mˆ2	90.85	6.37	0.33 m
Sage Creek	forelimb	0.51 m	0.041 mˆ2		6.40	0.08 m
Thalassomedon hanningtoni	forelimb	2.09 m	0.70 mˆ2		6.20	0.33m
Cryptoclidus oxoniensis	forelimb	0.63 m	0.11 mˆ2		3.45	0.18 m
Liopleurodon ferox	forelimb	70 pixels	1319 pixelˆ2		3.71	18.84 pixels
Nichollssaura borealis	forelimb	0.70 m	0.12 mˆ2		4.04	0.17 m
Parson's Creek	forelimb	1.26 m	0.34 mˆ2	100.39	4.61	0.27 m
Rhomaleosaurus thorntoni	forelimb	1.77 m	0.74 mˆ2		4.23	0.42 m
Tatenectes laramiensis	forelimb	0.67 m	0.10 mˆ2		4.50	0.14 m
Brancasaurus		1.03 m	0.20 mˆ2		5.19	0.2 m
Meyerosaurus		1.19 m	0.27 mˆ2		5.14	0.23 m
Trinacomerum osbornii		1.30 m	0.35 mˆ2	109.99	4.90	0.26 m
Average flapping angle				100.41		

Table A.4: Uncertainty range of reduced frequency of plesiosaurs as a function of flapping angle.

Flipper Type	Plesiosaur	Note	Flapping angle (deg)	Aspect ratio	Predicted Reduced frequency
High AR	*Albertonectes vanderveldei*	Exact value	90.85	6.37	0.108
	Sage Creek	Lower bound	109.99	6.4	0.089
		Average	100.41	6.4	0.097
		Upper bound	90.85	6.4	0.108
	Thalassomedon hanningtoni	Lower bound	109.99	6.2	0.092
		Average	100.41	6.2	0.101
		Upper bound	90.85	6.2	0.111
Low AR	*Cryptoclidus oxoniensis*	Lower bound	109.99	3.45	0.166
		Average	100.41	3.45	0.182
		Upper bound	90.85	3.45	0.201
	Liopleurodon ferox	Lower bound	109.99	3.71	0.154
		Average	100.41	3.71	0.168
		Upper bound	90.85	3.71	0.186
Moderate AR	*Nichollssaura borealis*	Lower bound	109.99	4.04	0.141
		Average	100.41	4.04	0.155
		Upper bound	90.85	4.04	0.171
	Parson's Creek	Exact value	100.39	4.61	0.136
	Rhomaleosaurus thorntoni	Lower bound	109.99	4.23	0.135
		Average	100.41	4.23	0.148
		Upper bound	90.85	4.23	0.164
	Tatenectes laramiensis	Lower bound	109.99	4.5	0.127
		Average	100.41	4.5	0.139
		Upper bound	90.85	4.5	0.153
	Brancasaurus	Lower bound	109.99	5.19	0.11
		Average	100.41	5.19	0.12
		Upper bound	90.85	5.19	0.133
	Meyerosaurus	Lower bound	109.99	5.14	0.111
		Average	100.41	5.14	0.121
		Upper bound	90.85	5.14	0.113
	Trinacomerum osbornii	Exact value	109.99	4.9	0.116

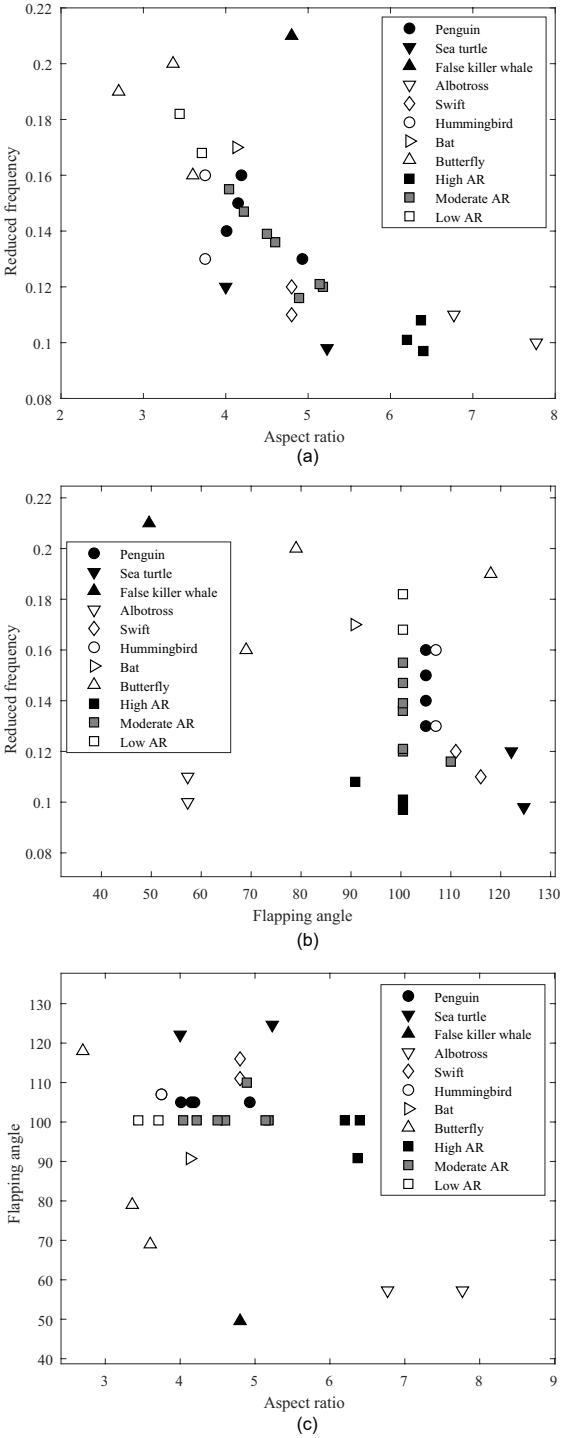

Figure A.3: Direct comparison between critical parameters for the specimens in Figure 2.4. (a) Relation between aspect ratio and reduced frequency. (b) Relation between flapping angle and reduced frequency. (c) Relation between aspect ratio and flapping angle.